THE JOURNAL OF BIOLOGICAL CHEMISTRY VOL. 286, NO. 43, pp. 37778–37792, October 28, 2011

Neuroprotection against Traumatic Brain Injury by a Peptide Derived from the Collapsin Response Mediator Protein 2 (CRMP2)*[S]

Received for publication, April 27, 2011, and in revised form, August 5, 2011 Published, JBC Papers in Press, August 9, 2011, DOI 10.1074/jbc.M111.255455

Joel M. Brittain[‡1], Liang Chen[§], Sarah M. Wilson[‡2], Tatiana Brustovetsky[¶], Xiang Gao[§], Nicole M. Ashpole[‡‖], Andrei I. Molosh[**], Haitao You[‡‡], Andy Hudmon[‡¶‖], Anantha Shekhar[§§], Fletcher A. White[‡¶¶‖‖], Gerald W. Zamponi[‡‡3], Nickolay Brustovetsky[‡¶], Jinhui Chen[‡§‖‖], and Rajesh Khanna[‡¶‖‖4]**

From the [‡]Program in Medical Neurosciences, Paul and Carole Stark Neurosciences Research Institute and the Departments of [§]Neurological Surgery, [¶]Pharmacology and Toxicology, [‖]Biochemistry and Molecular Biology, [**]Psychiatry, and [¶¶]Anesthesia, the [§§]Indiana Clinical and Translational Sciences Institute, and the [‖‖]Indiana Spinal Cord and Brain Injury Group, Indiana University School of Medicine, Indianapolis, Indiana 46202 and the [‡‡]Department of Physiology and Pharmacology, Hotchkiss Brain Institute, University of Calgary, Calgary, Alberta T2N 4N1, Canada

Background: CRMP2 is an axonal guidance protein that has been linked to NMDA receptor-mediated excitotoxicity.
Results: A CRMP2 peptide protects against NMDA receptor-mediated excitotoxicity *in vitro* and *in vivo* following a traumatic brain injury.
Conclusion: CRMP2 is a novel target for neuroprotection.
Significance: Targeting CRMP2 could lead to development of neurotherapeutics against traumatic brain injury as well as other neuronal insults.

Neurological disabilities following traumatic brain injury (TBI) may be due to excitotoxic neuronal loss. The excitotoxic loss of neurons following TBI occurs largely due to hyperactivation of *N*-methyl-D-aspartate receptors (NMDARs), leading to toxic levels of intracellular Ca^{2+}. The axon guidance and outgrowth protein collapsin response mediator protein 2 (CRMP2) has been linked to NMDAR trafficking and may be involved in neuronal survival following excitotoxicity. Lentivirus-mediated CRMP2 knockdown or treatment with a CRMP2 peptide fused to HIV TAT protein (TAT-CBD3) blocked neuronal death following glutamate exposure probably via blunting toxicity from delayed calcium deregulation. Application of TAT-CBD3 attenuated postsynaptic NMDAR-mediated currents in cortical slices. In exploring modulation of NMDARs by TAT-CBD3, we found that TAT-CBD3 induced NR2B internalization in dendritic spines without altering somal NR2B surface expression. Furthermore, TAT-CBD3 reduced NMDA-mediated Ca^{2+} influx and currents in cultured neurons. Systemic administration of TAT-CBD3 following a controlled cortical impact model of TBI decreased hippocampal neuronal death. These findings support TAT-CBD3 as a novel neuroprotective agent that may increase neuronal survival following injury by reducing surface expression of dendritic NR2B receptors.

Excitotoxic death of neurons occurs due to excessive Ca^{2+} influx, leading to activation of neurotoxic cascades (1). Ca^{2+} influx through NMDARs[5] is thought to be an integral mediator of excitotoxicity because antagonists of these receptors have been shown to be neuroprotective in animal models of traumatic brain injury (TBI) and ischemia-induced excitotoxicity (2, 3). However, the majority of human trials using NMDAR antagonists did not replicate the effectiveness seen in animal models and alarmingly found NMDAR antagonists to be toxic (4–7). In contrast, the non-competitive NMDAR antagonist memantine has shown early promise in various models of excitotoxicity (8, 9) and appears to be clinically well tolerated (10, 11). The limited successes of NMDAR antagonists emphasize a

* This work was supported, in whole or in part, by National Institutes of Health Grant R01 NS050131 (to N. B.). This work was also supported by a fellowship from the Alberta Heritage Foundation for Medical Research (AHFMR) (to H. Y.), American Heart Association National Scientist Development Grant SDG5280023 (to R. K.), a grant from the Indiana Clinical and Translational Sciences Institute funded, in part by a Project Development Team Grant Number RR025761 from the National Institutes of Health, National Center for Research Resources, Clinical and Translational Sciences Award (Indiana State Department of Health, Indiana Spinal Cord and Brain Injury Research Fund, Grants A70-0-079212 (to N. B.) and A70-9-079138 (to R. K.)), grants from the Ralph W. and Grace M. Showalter foundation (to A. H., N. B., and R. K.), and the Elwert Award in Medicine (to R. K.).
[S] The on-line version of this article (available at http://www.jbc.org) contains supplemental Figs. 1–4.
[1] Recipient of a Larry Kays Medical Neuroscience Fellowship.
[2] A Stark Scholar.
[3] An AHFMR Scientist and a Canada Research Chair, supported by the Canadian Institutes of Health Research.
[4] To whom correspondence should be addressed: 950 W. Walnut St., R2 Rm. 478, Indianapolis, Indiana 46202. Tel.: 317-278-6531; Fax: 317-278-5849; E-mail: khanna5@iupui.edu.

[5] The abbreviations used are: NMDAR, *N*-methyl-D-aspartate receptor; TBI, traumatic brain injury; ACSF, artificial cerebrospinal fluid; AP-5, (2*R*)-amino-5-phosphonopentanoate; CBD, CaV binding domain on CRMP2; CCI, controlled cortical impact; CPP, (±)-3-(2-carboxypiperazin-4-yl)propyl-1-phosphinic acid; ω-CTX, ω-conotoxin GVIA; DCD, delayed calcium deregulation; DIV, days *in vitro*; eEPSC, evoked excitatory post-synaptic current; FJB, Fluoro-Jade B; NR2B, NMDAR subunit 2B; SEP, superecliptic pHlourin; NR2B-SEP, NR2B fused to pH-sensitive GFP superecliptic pHlourin; TAT, transactivator of transcription domain; ANOVA, analysis of variance; E*n*, embryonic day *n*; *t*-Boc, 7-Amino-4-chloromethylcoumarin, t-Boc-Leu-Met (t-Boc-Leu-Met-CMAC); CGP 53432, 3[[(3,4-(dichlorophenyl)methyl]amino)-propyl] (diethoxymethyl)phosphinic acid; MTS, 3-(4,5-dimethylthiazol-2-yl)-5-(3-carboxymethoxyphenyl)-2-(4-sulfophenyl)-2H-tetrazolium.

need for development of new molecules that can protect neurons from excitotoxicity following stroke or TBI.

Recent findings suggest that the NMDAR-interacting collapsin response mediator protein 2 (CRMP2) may serve as a novel neuroprotective target (12, 13). CRMP2 is a cytosolic phosphoprotein that regulates axon guidance and outgrowth and has been implicated in various neurological disorders (14, 15). In addition to its role in axon growth, recent studies by our laboratory have characterized a novel role for CRMP2 in regulating synaptic transmission through interactions with Ca^{2+} channels (16–19). These biochemical and membrane trafficking studies demonstrated that CRMP2 modulates Ca^{2+} channel activity via alterations in surface expression. The newly discovered trafficking role of CRMP2 is the likely mechanism for the changes observed in Ca^{2+} channel activity following alteration of CRMP2 expression (16–19).

CRMP2 was first implicated in ischemia when an atypical molecular weight isoform of CRMP2 appeared in rat brain tissue following middle carotid artery occlusion (20) and was found to be up-regulated following focal cerebral ischemia (21). Later studies identified that the cleavage was by calpain (13, 22–26), a Ca^{2+}-activated protease that has been heavily linked to neurotoxic signaling (27). The cleavage of CRMP2 by calpain occurs following ischemia (23), neurotrauma (26), excitotoxicity (13), and nerve growth factor deprivation-induced neurite degeneration (24). This cleavage is not specific to CRMP2, however, because CRMP1, -3, -4, and -5 also appear to be cleaved by calpain following neurotoxic insult (23, 26, 28). In the present study, we demonstrate that a CRMP2 peptide down-regulates dendritic surface expression of NMDARs and protects against neurotoxicity in cell-based assays and in TBI.

EXPERIMENTAL PROCEDURES

Materials—TAT-Control (YGRKKRRQRRRWEAKEMLYFEALVIE (TAT sequence denoted by the underline); a random sequence with no homology to any known sequence) and TAT-CBD3 (YGRKKRRQRRRARSRLAELRGVPRGL) were synthesized by Antagene Inc. (Sunnyvale, CA). All chemicals unless otherwise noted were purchased from Sigma. Lipofectamine 2000 was purchased from Invitrogen. Fura-2/AM and Fura-2FF/AM were obtained from Teflabs (Austin, TX). Antibodies were purchased as follows: rabbit anti-CRMP2 (Sigma), mouse anti-αII-spectrin clone AA2 (Millipore, Billerica, MA), mouse anti-NR2B (BD Biosciences), mouse anti-Kv2.1 clone K89/34 (University of California Davis/National Institutes of Health NeuroMab Facility, Davis, CA), and mouse anti-β-tubulin III (Promega, Madison, WI).

Cell Preparation and Culture—Pregnant Sprague-Dawley rats were purchased from Harlan Laboratories (Indianapolis, IN). Cortical neurons were isolated from embryonic day 18–19 (E18–19) pups and cultured as described previously (16). Neurons were cultured on poly-D-lysine-coated plates or coverslips.

Excitotoxicity Stimulation by Glutamate/Glycine—E18–19 cortical neurons (grown for 7 days *in vitro* (DIV)) in 12-well dishes on coverslips were treated with 200 μM glutamate, 20 μM glycine or control medium for 1 h at 37 °C. Cells were stained using Live/Dead cytotoxicity/viability kit (Invitrogen) staining at 24 h following stimulation. Briefly, coverslips were incubated for 40 min at room temperature, washed three times in PBS, and immediately imaged on a Nikon Ti-E inverted microscope. Each coverslip was imaged in three different fields using a Texas Red filter to detect cytotoxic neurons and a fluorescein isothiocyanate (FITC) filter to detect viable neurons. Neurons were quantified using the automated counting software Nikon Elements 3.0. Total neuron number was determined by the addition of cytotoxic and viable cells. Total cell number between control and treatment groups was compared, and no statistical significance was found. Vehicle (0.05% DMSO) or peptides were incubated for 20 min prior to the addition of glutamate/glycine.

Excitotoxicity Stimulation by Glutamate/D-Serine—E18–19 cortical neurons (7–8 DIV) grown in 96-well plates were stimulated for 30 min in serum-free medium in a final volume of 100 μl. The excitotoxic insult was achieved by the addition of 200 μM L-glutamate and 100 μM D-serine (an NMDAR co-agonist (29)). Following stimulation, all medium was removed from neurons and replaced with fresh complete medium. Cells were grown for 24 h under normal growth conditions before cell viability was measured. The cell viability of cultured neurons was quantified using the CellTiter 96® AQ_{ueous} One Solution Cell Proliferation Assay (MTS) from Promega. Following the 24-h growth period, MTS reagent was added to each well and incubated for 1 h at 37 °C. MTS is a tetrazolium analog that is converted to the water-soluble blue absorbing formazan by the endogenous reductases of living cells (30). The formation of formazan following incubation with MTS reagent was then measured (*Viktor3v*, PerkinElmer Life Sciences) by recording the absorbance at 490 nm. Control wells containing medium only (no cells) were used to subtract the background absorbance from the neuronal culture medium.

Lentivirus-mediated CRMP2 Knockdown—Lentiviral particles containing expression constructs for scramble shRNA or CRMP2 shRNA sequences were generated as described previously (16). Cortical neurons grown for 2 DIV were transduced with lentiviral particles (~1.45×10^{10}/well of a 96-well plate) and used for experiments 5 days later.

In Vitro Calpain Cleavage and Immunoblotting—Lysates were freshly prepared from E18–19 brains using a mild lysis buffer (20 mM Tris-HCl, pH 7.5, 5 mM $MgCl_2$, 150 mM NaCl, 1 mM EDTA, 0.1% Nonidet P-40). Briefly, rat brains were homogenized and then allowed to lyse for 30 min before clarifying by centrifugation at 15,000 × *g* for 20 min. The soluble protein fraction was removed and used the same day for cleavage experiments. Lysates were incubated with TAT-CBD3 or MDL28170 for 10 min prior to the addition of 20 mM $CaCl_2$. Lysates were then incubated at room temperature for 30 min to allow for proteolytic cleavage. Reactions were stopped by the addition of SDS loading buffer and then processed for immunoblotting. Immunoblotting was performed as previously described (16, 17).

In Vitro Measurement of Calpain Activity—Lysates were prepared as described above and incubated for 10 min with vehicle (0.2% DMSO), TAT-CBD3 (10 μM), or MDL-28170 (50 μM) prior to the addition of 20 mM $CaCl_2$. The fluorogenic calpain substrate 7-Amino-4-chloromethylcoumarin, t-Boc-Leu-Met (t-Boc-Leu-Met-CMAC) (*t*-Boc; 10 μM) was then added to the

lysates. Samples were then transferred to a 96-well plate and incubated for 30 min at 37 °C. Cleavage of *t*-Boc was assayed by measuring fluorescence using a plate reader (*Viktor3v*, PerkinElmer Life Sciences) with a 355-nm excitation filter and a 460-nm emission filter (31). Wells containing *t*-Boc alone were used to subtract background fluorescence. Background-subtracted values were then normalized to vehicle-treated samples.

Biotinylation of Neuronal Cultures—This was performed as described (16, 17). Neurons were kept at 4 °C throughout the biotinylation and lysis procedures. Neurons were washed three times with ice-cold PBS (pH 7.5) prior to being incubated with 1 mg/ml biotin (EZ-Link® sulfosuccinimidyl-6-[biotin-amido]-hexanoate (Sulfo-NHS-LC-Biotin), Thermo Scientific) in PBS, pH 7.5, for 30 min in the dark. Neurons were then washed once with PBS (pH 7.5) and incubated with 100 mM glycine in PBS for 1 min to chelate excess biotin. Cells were then washed twice with PBS before lysis. Cells were lightly resuspended in cold PBS and then centrifuged at 15,000 × *g* for 2 min at 4 °C. The pelleted cells were resuspended and lysed in radioimmune precipitation lysis buffer (50 mM Tris-HCl, pH 8, 1% Nonidet P-40, 150 mM NaCl, 0.5% sodium deoxycholate, and 1 mM EDTA, supplemented with freshly added protease inhibitors: 1 μg/ml leupeptin, 2 μg/ml aprotinin, 1 mM phenylmethylsulfonyl fluoride (Sigma) together with a protease inhibitor mixture (G Biosciences, Maryland Heights, MO)). Samples were centrifuged at 15,000 × *g* for 20 min to clarify the lysate. The protein concentration of all samples was determined by BCA protein assay (Thermo Scientific). After normalizing all samples to protein content, equal volumes were added to 37.5 μl of streptavidin-agarose (Thermo). Lysates were incubated overnight at 4 °C with continual agitation and then washed four times with radioimmune precipitation buffer before boiling in SDS loading buffer. Immunoblotting was performed as described (16).

Calcium Imaging—Cortical neurons were loaded at 37 °C with 2.6 μM Fura-2FF/AM (K_d = 25 μM, λ_{ex} = 340, 380 nm/λ_{em} = 512 nm) to follow changes in cytosolic Ca^{2+} ($[Ca^{2+}]_c$) in a standard bath solution containing 139 mM NaCl, 3 mM KCl, 0.8 mM $MgCl_2$, 1.8 mM $CaCl_2$, 10 mM NaHEPES, pH 7.4, 5 mM glucose. Fluorescence imaging was performed with an inverted microscope (Nikon Eclipse TE2000-U), using objective Nikon Super Fluor 20×, 0.75 numerical aperture and a Photometrics cooled CCD camera $CoolSNAP_{HQ}$ (Roper Scientific, Tucson, AZ) controlled by MetaFluor 6.3 software (Molecular Devices, Sunnyvale, CA). The excitation light was delivered by a Lambda-LS system (Sutter Instruments, Novato, CA). The excitation filters (340 ± 5 and 380 ± 7 nm) were controlled by a Lambda 10-2 optical filter change (Sutter Instruments). Fluorescence was recorded through a 505-nm dichroic mirror at 535 ± 25 nm. To minimize photobleaching and phototoxicity, the images were taken every 15 s during the time course of the experiment using the minimal exposure time that provided acceptable image quality. The changes in $[Ca^{2+}]_c$ were monitored by following a ratio of F340/F380, calculated after subtracting the background from both channels. $[Ca^{2+}]_c$ was calculated using the Grynkiewicz equation using K_D = 25 μM for Fura-2FF and K_D = 224 nM for Fura-2 (32).

Whole Cell Patch Clamp Recordings from Cortical Neurons in a Slice Preparation—The brains of anesthetized Sprague-Dawley rats (~100 g) were rapidly dissected, and coronal slices (350-μm thickness) were obtained as described earlier (33, 34). Slices were immersed in an oxygenated (mixture of 95% oxygen and 5% carbon dioxide) artificial cerebrospinal fluid (ACSF) of the following composition: 130 mM NaCl, 3.5 mM KCl, 1.1 mM KH_2PO_4, 1.3 mM $MgCl_2$, 2.5 mM $CaCl_2$, 10 mM glucose, 30 mM $NaHCO_3$ at room temperature for at least 1 h prior to recording. Slices were then transferred to a submersion-type slice chamber mounted on the stage of a Nikon E600FN Eclipse microscope (Nikon Instruments Inc., Melville, NY) and perfused at rate of 2–3 ml/min with ACSF heated to 30 °C. Whole cell patch clamp recordings were obtained using standard techniques with borosilicate glass electrodes (resistance 3–6 megaohms, WPI, Sarasota, FL) filled with a potassium gluconate-based recording solution with the following composition: 140 mM potassium gluconate, 2 mM KCl, 3 mM $MgCl_2$, 10 mM HEPES, 5 mM phosphocreatine, 2 mM potassium-ATP, 0.2 sodium-GTP) adjusted to pH 7.3 with KOH, and having an osmolarity of 285–295 mosM.

Individual cortical neurons were visualized *in situ* using differential interference contrast microscopy in combination with a 40× water immersion objective and displayed in real time on a monitor. Whole cell recordings were made with a Multiclamp 700B amplifier (Molecular Devices) using pClamp 10.2 software and a Digidata 1322A interface (Molecular Devices). Drugs were applied by adding them at the required concentration directly into the ACSF. To examine the effects of TAT-CBD3 on stimulus-evoked postsynaptic currents, a concentric stimulating electrode (FHC, Bowdoinham, ME) was placed ~500 μm from the recorded neuron. A stimulus was repeated five times at a frequency of 0.2 Hz and then averaged for subsequent data analysis. For comparison between control and peptide states, all data were normalized to the mean of the last two data points acquired immediately before the onset of TAT-CBD3 application (~4 min of control data). Evoked excitatory postsynaptic currents (eEPSCs) were accepted as being monosynaptic if the response latency was below 4 ms. The eEPSCs were elicited from a holding potential of −60 mV. To isolate compound glutamate receptor-mediated eEPSCs, SR 95531 (5 μM) and CGP 53432 (1 μM) were applied throughout the experiments to block inhibitory $GABA_A$ and $GABA_B$ transmission, respectively. To isolate NMDA receptor-mediated eEPSCs, the AMPA/kainate receptor antagonist 6,7-dinitroquinoxaline-2,3-(1H,4H)-dione (10 μM) was included in the SR 95531- and CGP 53432-containing ACSF. At the end of each isolated eEPSC experiment, the NMDA antagonist (±)-3-(2-carboxypiperazin-4-yl)propyl-1-phosphinic acid (CPP; 1 μM) was added to the ACSF. All drugs were purchased from Sigma except for CGP 53432, CPP, and SR 95531, which were obtained from Tocris Cookson Inc. (Ellisville, MO). Access resistance was continuously monitored throughout by injection of a transient (50-ms) voltage step (−3 mV) immediately prior to the beginning of each stimulation pulse.

Superecliptic pHlourin (SEP) Fluorescent Microscopy—E18–19 cortical neurons, transfected with NR2B-SEP DNA using Lipofectamine (16), were imaged on a Nikon Ti swept

field confocal microscope using a 60×, 1.4 numerical aperture lens and a standard fluorescein isothiocyanate cube with a cooled Cascade 512B digital camera (Photometrics, Tucson, AZ). Neuronal somatic fluorescence was measured by digital video microfluorometry with an intensified CCD camera coupled to a microscope and Nikon Elements Software (Nikon Instruments Inc.). Cells were bathed, and all drugs were diluted in extracellular solution (140 mM NaCl, 10 mM HEPES, 2 mM $CaCl_2$, 1 mM $MgCl_2$, 10 mM glucose, 5 mM KCl, pH 7.4). Experiments were completed at room temperature, and images were taken every 15 s (spines) or 10 s (soma) to prevent photobleaching. After completing each imaging experiment, SEP fluorescence was quenched by the addition of acetic acid. Finally, cellular integrity was verified by differential image contrast microscopy.

Transfection of Cortical Neurons with CRMP-2 siRNA—Cortical neurons grown for 5 DIV were transfected with 200 nM CRMP-2 siRNA and 0.1 μg of enhanced green fluorescent protein DNA using Lipofectamine 2000 as described previously (16, 19).

Hippocampal Neuron Whole Cell Voltage Clamp Electrophysiology—Whole cell voltage clamp recordings were performed on rat hippocampal neurons (DIV 7–11) days in culture (35), at room temperature using an Axopatch 200B amplifier (Axon Instruments, Union City, CA), with a holding potential of −60 mV. The external solution contained 140 mM NaCl, 5 mM KCl, 1 mM $CaCl_2$, 25 mM HEPEs, and 33 mM D-glucose, pH adjusted to 7.4 with NaOH. The external solution was supplemented with 0.5 μM tetrodotoxin (TTX) (Tocris Bioscience), 100 μM picrotoxin, 100 μM glycine. The internal pipette solution was composed of 120 mM CsCl, 35 mM CsOH, 11 mM EGTA, 1 mM $CaCl_2$, 2 mM $MgCl_2$, 10 mM HEPES, 4 mM ATP (Tris salt), 20 mM phosphocreatine (Tris salt), and creatine phosphokinase (50 units/ml), pH adjusted to 7.3 with CsOH.

Drug delivery was controlled by a Valvelink8.2 perfusion system (Automate Scientific Inc., Berkeley, CA) with a pressurized superfusion device to achieve fast switching of solution. NMDA current was evoked by application of NMDA (50 μM; Tocris Bioscience) for 2 s every 30 s. During experiments, control NMDA current was stabilized for 5 min (10 traces, with peak current fluctuation within 5%) before TAT-CBD3 application. Data were analyzed using Clampfit (Axon Instruments), Origin 7 (OriginLab, MA), and Prism 5 (GraphPad Software Inc., San Diego, CA).

Animals Used for TBI—Male C57BL/6 mice (The Jackson Laboratories) were group-housed with a 12/12-h light/dark cycle with access to food and water *ad libitum*. All procedures were performed under protocols approved by the Animal Care and Use Committee of Indiana University.

Controlled Cortical Impact (CCI) Model of TBI—C57BL/6 male (8-week-old) mice were subjected to moderate CCI injury as described previously (36–38) with the following modifications. The deformation impact depth was set at 1.0 mm, and the piston velocity was controlled at 3.0 m/s; these modifications result in a moderate level of injury using an electromagnetic model (39). Briefly, the mice were anesthetized with avertin and placed in a stereotaxic frame (Kopf Instruments, Tujunga, CA) prior to TBI. Using sterile procedures, the skin was retracted, and a 4-mm craniotomy centered between the lambda and bregma sutures was performed. A point was identified midway between the lambda and bregma sutures and midway between the central suture and the temporalis muscle laterally. The skullcap was carefully removed without disruption of the underlying dura. Prior to the injury, the head of the animal was angled on a medial to lateral plane so that the impacting tip was perpendicular to the exposed cortical surface. This was accomplished by rotating the entire stereotaxic frame on the transverse plane. The mouse CCI model uses an electromagnetic model (39) with which the experimenter can independently control the contact velocity and the level of cortical deformation, thus altering the severity of the injury. During all surgical procedures and recovery, the core body temperatures of the animals were maintained at 36–37 °C.

TAT-CBD3 Administration—TAT-CBD3 was prepared in sterile saline immediately prior to use. TAT-CBD3 (20 mg/kg body weight) was injected intraperitoneally 5 min after the injury. An equal volume of saline was injected as the vehicle control into mice that had also undergone CCI and surgery.

Tissue Processing—At 24 h after TBI surgery, animals were deeply anesthetized with an overdose of avertin and then perfused transcardially with ice-cold 0.9% saline, followed by a fixative containing 4% paraformaldehyde in PBS. The brains were removed and post-fixed in paraformaldehyde overnight and then cryoprotected with 30% sucrose for 48 h. Serial coronal sections (30 μm thick) were cut using a cryostat (Microm HM 500 M) and stored at −20 °C. The sections were then processed for Fluoro-Jade B staining.

Fluoro-Jade B (FJB) Staining, Microscopy, and Quantification—The staining procedures were implemented as described previously (40). Briefly, sections were first incubated in a solution of 1% alkaline (NaOH) in 80% ethanol for 5 min and then hydrated in 70% ethanol for 2 min followed by distilled water for 5 min. The sections were then sequentially incubated in a solution of 0.06% potassium permanganate for 20 min, rinsed in distilled water for 2 min, incubated in a 0.0004% solution of FJB (Histo-Chem Inc., Jefferson, AR) for 20 min, and counterstained with DAPI (Sigma) for 5 min. Finally, sections were rinsed in distilled water and air-dried overnight. The dry slides were mounted with Distrene-80 (DPX) (Fluka).

The sections were analyzed by fluorescence microscopy at a primary magnification of ×10–63 with an inverted microscopy system (Zeiss Axiovert 200 M, Carl Zeiss MicroImaging, Inc., Thornwood, NY) interfaced with a digital camera (Zeiss Axio Cam MRc5, Carl Zeiss MicroImaging, Inc.). Images were captured with imaging software (AxioVision, version 4.0, Carl Zeiss MicroImaging, Inc.) and assembled and labeled with Photoshop 7.0 (Adobe Systems, Adobe Systems Inc., San Jose, CA).

After sectioning, one section of every six throughout the entire extent of the hippocampal formation (from bregma −0.94 to −3.80 mm) was selected for assessment with FJB staining. The anatomical boundaries of hippocampus and each hippocampal subregion (CA1, CA3, granular cell layer, molecular cell layer; and hilus) were identified as described by Amaral and Witter (41). Their area (in μm^2) was measured with imaging software (AxioVision, version 4.0, Carl Zeiss MicroImaging, Inc.) and calculated with the section thickness. The total num-

ber of FJB-positive neurons was determined through a double-blinded quantitative histological analysis under a microscope system (Zeiss Axiovert 200 M, Carl Zeiss MicroImaging, Inc.) with a ×40 objective. The density of FJB-positive cells was presented as number/mm^3.

Statistical Analyses—All results are presented as mean ± S.E. values. Experimental values were compared using Student's *t* test or one-way analysis of variance (ANOVA) and *post hoc* Dunnett's test. Values were considered statistically significant at $p < 0.05$.

RESULTS

TAT-CBD3, a CRMP2-derived Peptide Prevents against Glutamate-induced Cell Death—We recently identified a Ca^{2+} channel-binding domain on CRMP2 (*i.e.* CBD3) that exhibited binding to and regulated function of voltage-gated calcium channels (16). A potential importance of this domain in CRMP2-mediated Ca^{2+} signaling can be inferred from the observation that the Ca^{2+}-binding protein calmodulin apparently shields CRMP2 from calpain cleavage by binding N-terminal to the CBD3 sequence (25, 26). Due to the proximity of CBD3 to putative calpain cleavage sites that are slightly more C-terminal (26) to CBD3, we hypothesized that the CBD3 peptide could alter calpain-mediated cleavage of CRMP2 and thus may have neuroprotective effects. To facilitate CBD3 entry into neurons, we fused it to the protein transduction domain of HIV-1 TAT protein (42), yielding TAT-CBD3. The cell penetration ability of this peptide was monitored using an FITC-labeled version of TAT-CBD3 that exhibited robust accumulation into E18–19 cortical neurons within 5 min of incubation (supplemental Fig. 1). To determine if CBD3 is neuroprotective, we tested TAT-CBD3 in models of glutamate-induced toxicity. Neurons cultured for 7–8 DIV were pretreated for 20 min with either vehicle (DMSO) or TAT peptides and then stimulated for 1 h with 200 μM glutamate + 20 μM glycine, and cell death was quantified 24 h later (Fig. 1*A*). Neuronal death was quantified using a Live/Dead cytotoxicity/viability assay, wherein live cells are identified by calcein fluorescence and dead cells by fluorescence of ethidium homodimer-1 following binding to DNA (Fig. 1, *B–E*). Stimulated neurons exhibited 34.4 ± 2.0% ($n = 7$) cell death compared with 8.6 ± 0.8% death in control neurons ($n = 5$). Incubation with 10 μM TAT-CBD3 abolished glutamate-induced increase in cell death (9.6 ± 0.5%, $n = 6$; Fig. 1*F*). Incubation with TAT-Control peptide exhibited no change in cell death (35.7 ± 2.2%, $n = 6$) compared with stimulated neurons treated with DMSO. A dose-response curve was constructed to determine the IC_{50} for neuroprotection by TAT-CBD3 (Fig. 1*G*). These data were fitted to a sigmoidal dose-response function (see "Experimental Procedures"), yielding an IC_{50} value of 1.95 ± 0.23 μM ($n = 5–6$). Because 10 μM yielded a maximum reduction in cell death and is ~5-fold the calculated IC_{50}, 10 μM TAT-CBD3 was used for all subsequent experiments unless otherwise noted.

TAT-CBD3 Increases Cell Viability following an Excitotoxic Insult—The neuroprotective action of TAT-CBD3 was further tested using an alternative stimulation protocol along with measuring cell viability instead of cell death. Neurons were pretreated for 10 min with TAT peptides and then stimulated for 30 min with 200 μM glutamate and 100 μM D-serine; D-serine has been reported to be the dominant co-agonist for glutamate toxicity (29, 43). Cell viability was measured 24 h later by an MTS cell viability assay, which measures reductase activity in metabolically active cells. Within each experiment, cell viability values were normalized to values obtained for unstimulated control neurons. Approximately 58 ± 4% of the neurons survived the Glu/Ser stimulation compared with unstimulated neurons (Fig. 2*A*). Notably, the level of cell death observed in this excitotoxic paradigm (~40%) is consistent with the ~35% cell death observed with the Glu/Gly stimulation described above. Neurons pretreated for 10 min with 10 μM TAT-CBD3 and then stimulated with Glu/Ser completely survived the excitotoxic treatment. Significant neuroprotection by TAT-CBD3 was evident at 3 and 1 μM but not at 0.1 μM. In contrast, pretreating neurons with 10 μM TAT-Control resulted in cell viability levels (~59 ± 5%, $n = 48$) similar to Glu/Ser-stimulated neurons. Treatment of neurons with 10 μM TAT-CBD3 alone,

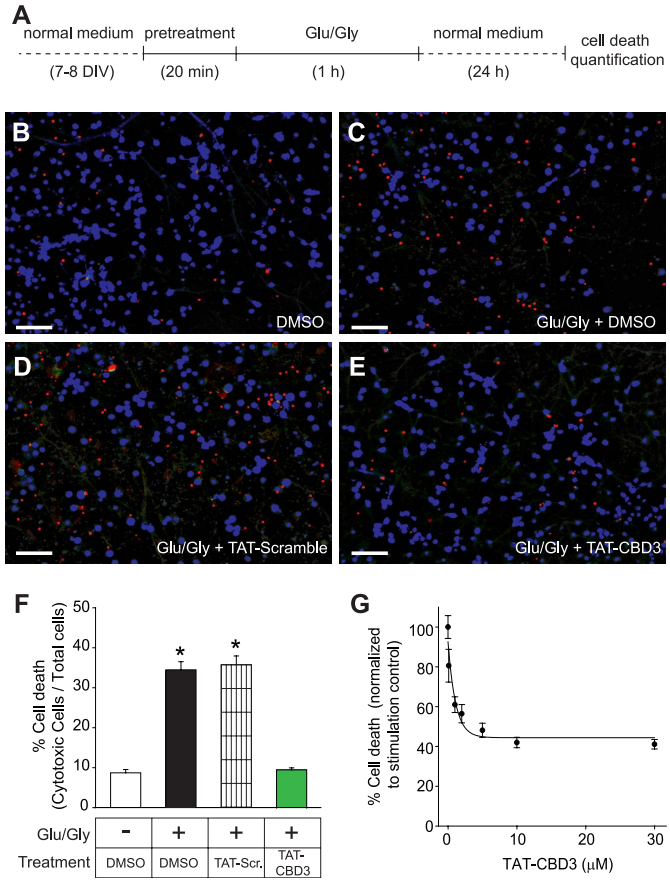

FIGURE 1. **Prevention of excitotoxic death with TAT-CBD3.** *A*, E18–19 cortical neurons grown for 7 DIV were treated with 200 μM glutamate plus 20 μM glycine or control medium for 1 h at 37 °C and then stained 24 h later with a Live/Dead cytotoxicity/viability assay (Molecular Probes) and immediately imaged. *B–E*, representative images of cytotoxic cells (*red*) and viable cells (*blue*); *scale bar*, 100 μm. Twenty min before stimulation, the neurons were treated with DMSO control (*C*), TAT-Control (*D*), or TAT-CBD3 (*E*). Average death in each coverslip was counted in three fields. The percentage death of 5–7 coverslips is represented as S.E. (*error bars*) ($n = 5–7$ for each condition) (*F*). One-way ANOVA with *post hoc* Dunnett's test indicated significant differences compared with control or TAT-CBD3-treated groups; *, $p < 0.05$. *G*, average cell death with varying concentrations of TAT-CBD3 pretreatment. Death is normalized to glutamate/glycine stimulation. The IC_{50} of TAT-CBD3 was determined by fitting the curve to a four-parameter logarithmic function.

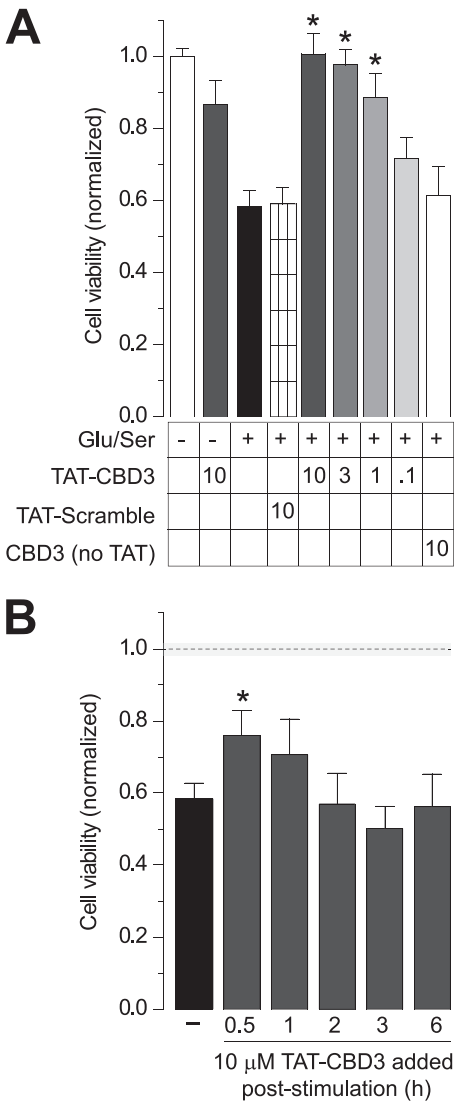

FIGURE 2. **Prevention of glutamate-induced reduction in cell viability by TAT-CBD3.** *A*, cell viability of E18–19 DIV 7 cortical neurons was determined using an MTS cell viability assay. Neurons were incubated with peptides for 10 min prior to stimulation with 200 μM glutamate and 100 μM D-serine for 30 min. Viability was then measured 24 h later, with all values normalized to no stimulation control ($n \geq 32$ each from at least four separate experiments). *, significant difference compared with stimulated control ($p < 0.05$). All values are in μM. *B*, viability of stimulated neurons was also measured with the addition of TAT-CBD3 at various time points following stimulation ($n \geq 16$). *, S.D. compared with stimulated control ($p < 0.05$). The *dotted line* and *shaded area* around the line illustrate the normalized cell viability ± S.E. in the absence of any stimulation (from *A*). *Error bars*, S.E.

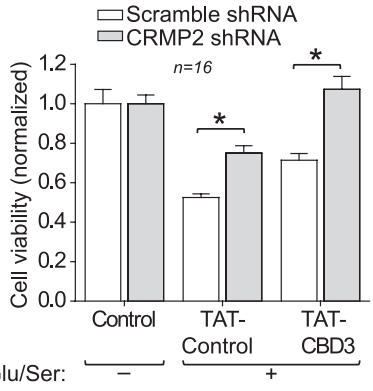

FIGURE 3. **CRMP2 knockdown is neuroprotective.** E18–19 neurons grown for 2 DIV were incubated with 1.45×10^{10} lentiviral particles for 5 days and then stimulated with 200 μM glutamate and 100 μM D-serine for 30 min. Cell viability was measured 24 h later with the MTS assay, with all values normalized to no stimulation control. Knockdown of CRMP2 significantly increased cell viability in the face of an excitotoxic challenge (*, $p < 0.05$ *versus* control shRNA; Student's *t* test). Neurons infected with CRMP2 shRNA and then additionally incubated with TAT-CBD3 peptide for 10 min prior to stimulation showed compete resistance to cell death (*, $p < 0.05$ *versus* control shRNA; Student's *t* test). *Error bars*, S.E.

without stimulation, did not affect cell viability. Application of a CBD3 peptide lacking the TAT cell-penetrating sequence did not protect cells from Glu/Ser-induced cell death, suggesting that the CBD3 peptide acts on an intracellular target to achieve neuroprotection.

An important aspect of neuroprotective agents is their ability to prevent excitotoxic death when administered poststimulation. To test if TAT-CBD3 is neuroprotective following stimulation, neurons were treated with 10 μM TAT-CBD3 for 10 min at 0.5, 1, 2, 3, and 6 h after Glu/Ser stimulation, and cell viability was measured as described. Except for modest, but statistically significant, neuroprotection at 0.5 h following stimulation (Fig. 2*B*), TAT-CBD3 was not effective at later times. Together, the results suggest that 1) TAT-CBD3 is neuroprotective, and 2) the interaction between CRMP2 and target protein is probably important for mediating the early phase of neuronal death observed following excitotoxic insults.

Lentivirus-mediated Knockdown of CRMP2 Is Neuroprotective—Our initial findings show that TAT-CBD3 protects neurons from an excitotoxic insult but raise some important questions: 1) is the neuroprotection due to inhibition specifically of CRMP2, and 2) does the activity of TAT-CBD3 require CRMP2 to be present? To address if the neuroprotection was due to CRMP2, we reduced endogenous CRMP2 expression by transducing cortical neurons with lentiviral particles containing shRNA targeting CRMP2 or a scramble shRNA sequence at 2 DIV, a viral knockdown approach that knocks down >85% of CRMP2, as reported by us previously (16). After 5 days, the lentivirus-transduced neurons were pretreated with TAT peptides for 10 min and then stimulated with Glu/Ser, and cell viability was measured 24 h later (Fig. 3). Cell viability was normalized to control neurons (no stimulation) treated with the same virus (scramble *versus* CRMP2 shRNA). CRMP2 shRNA lentivirus-transduced neurons exhibited a significant increase in cell viability following stimulation compared with scramble shRNA-treated neurons when pretreated with TAT-Control (0.75 ± 0.04 *versus* 0.52 ± 0.02, $p < 0.05$, Student's *t* test, $n = 16$). Complete neuroprotection was observed in neurons transduced with CRMP2 shRNA lentivirus and pretreated with TAT-CBD3 prior to excitotoxic challenge (1.07 ± 0.07; $n = 16$). That neurons transduced with scramble shRNA lentivirus did not exhibit complete neuroprotection with TAT-CBD3 (*e.g.* compared with ~100% protection in TAT-CBD3-treated cells; Fig. 2*A*) can probably be attributed to the alteration of survival by the viral load itself. Nonetheless, these findings demonstrate that it is CRMP2 itself that mediates the neuroprotection. Furthermore, because TAT-CBD3 is also neuroprotective, it is likely that TAT-CBD3 works through antagonizing a function of CRMP2.

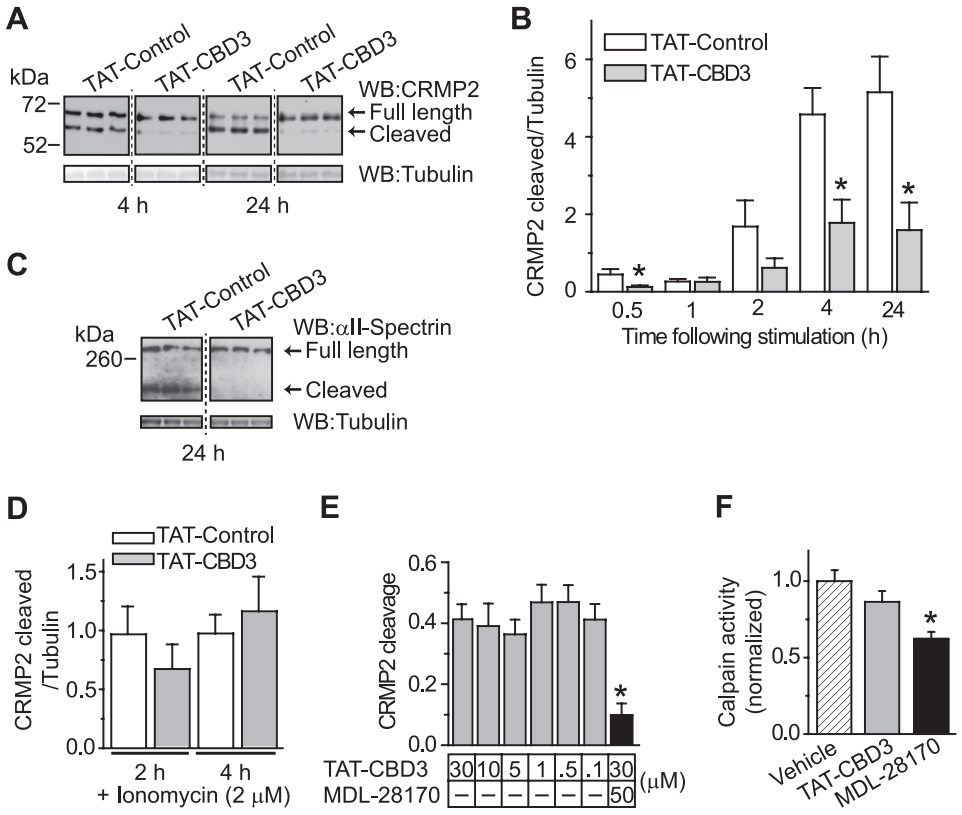

FIGURE 4. **TAT-CBD3 decreases glutamate-induced cleavage of CRMP2.** *A*, Western blot (*WB*) of CRMP2 cleavage following excitotoxic challenge. E18–19 DIV 7 neurons were stimulated with Glu/Ser for 30 min, and lysates were prepared 4 and 24 h later. Cleavage of CRMP2 is observed by the appearance of a ~55 kDa band representing cleaved CRMP2. Tubulin loading controls are also shown. *B*, summary of CRMP2 cleavage at various times following stimulation. Cleavage of CRMP2 is presented as cleaved CRMP2/tubulin ($n = 6$–12/condition). *, significant difference compared with time-matched TAT-Control ($p < 0.05$; Student's *t* test). *C*, αII-spectrin cleavage at 24 h following glutamate stimulation in the presence of TAT-Control or TAT-CBD3, along with tubulin loading control ($n = 6$). *D*, CRMP2 cleavage following either 2- or 4-h exposure to 2 μM Ca^{2+} ionophore ionomycin ($n = 8$–9). *E*, equal amounts of lysates prepared from E18–19 brains were treated for 10 min with TAT-CBD3 (0.1–30 μM) or 30 μM TAT-CBD3 + 50 μM MDL28170, and then calpain activity was activated by the addition of 20 mM $CaCl_2$. The cleavage reaction was stopped at 30 min, and CRMP2 cleavage was assessed by immunoblotting. TAT-CBD3 did not affect *in vitro* cleavage of CRMP2, whereas MDL28170 completely prevented CRMP2 cleavage (*, $p < 0.05$ *versus* all other conditions; $n = 4$–5/condition). For these experiments, CRMP2 cleavage represents cleaved CRMP2/total CRMP2. *F*, lysates were preincubated with vehicle (0.1% DMS), TAT-CBD3 (10 μM), or MDL-28170 (50 μM) prior to measuring calpain activity via measurement of cleavage of the fluorogenic calpain substrate *t*-Boc (*, $p < 0.05$ *versus* vehicle by one-way ANOVA with *post hoc* Dunnett's test; $n = 23$–24 from three experiments). *Error bars*, S.E.

TAT-CBD3 Reduces Calpain Cleavage of CRMP2—CRMP2 is cleaved by the protease calpain following various types of neurotoxic insults, including injury, ischemia, and excitotoxic exposure to glutamate (13, 20, 22–24, 26). By virtue of its proximity to calpain cleavage sites on CRMP2, CBD3 could directly affect CRMP2 cleavage. Alternatively, CBD3 could inhibit calpain-dependent cleavage of CRMP2 by inhibiting Ca^{2+} influx required for calpain activation. Thus, we asked if TAT-CBD3 could alter calpain cleavage of CRMP2 following glutamate- or ionomycin-induced activation of calpain (44). Lysates from 7 DIV neurons were subjected to a 30-min Glu/Ser stimulation and immunoblotted with a CRMP2 antibody that recognizes C-terminal cleaved and full-length CRMP2. Blots were also probed for β-tubulin, which served as a loading control. We observed a 55-kDa cleaved fragment of CRMP2 as well as the 62-kDa full-length CRMP2 protein (Fig. 4*A*), consistent with earlier findings (13, 22). CRMP2 cleavage was quantified by densitometry and is reported as the ratio of cleaved CRMP2 to tubulin (Fig. 4*B*). Exposing neurons to 10 μM TAT-CBD3 prior to stimulation led to a significant reduction in CRMP2 cleavage at 0.5, 4, and 24 h following stimulation compared with neurons treated with 10 μM TAT-Control ($p < 0.05$, Student's *t* test, $n = 6$–12). For example, at 24 h poststimulation, neurons exposed to TAT-CBD3 had ~70% less cleaved CRMP2 compared with neurons exposed to TAT-Control.

In addition to CRMP2, we also observed that cleavage of the prototypical calpain substrate αII-spectrin (45) was inhibited by TAT-CBD3 (Fig. 4*C*). Cleavage resulting from nonspecific influx of Ca^{2+} into neurons following challenge with the Ca^{2+} ionophore ionomycin, which has been shown to activate calpain (46), was not affected by TAT-CBD3 (Fig. 4*D*). TAT-CBD3 also did not affect CRMP2 cleavage in lysates, ruling out the possibility that CBD3 is directly inhibiting calpain (Fig. 4*E*). Consistent with these results, calpain activity (measured in lysates using the fluorogenic calpain substrate *t*-Boc) was not affected by incubation with TAT-CBD3 (Fig. 4*F*). Collectively, these findings suggest that that TAT-CBD3 does not prevent CRMP2 cleavage due to direct modulation of calpain or CRMP2 *per se*; rather, it appears that TAT-CBD3 acts on a target upstream of calpain activation.

TAT-CBD3 Reduces Glutamate-stimulated Ca^{2+} Influx—The neuroprotective effect of TAT-CBD3 prior to but not following Glu/Ser stimulation suggests that the mode of action of TAT-CBD3 may occur early in the glutamate toxicity pathway.

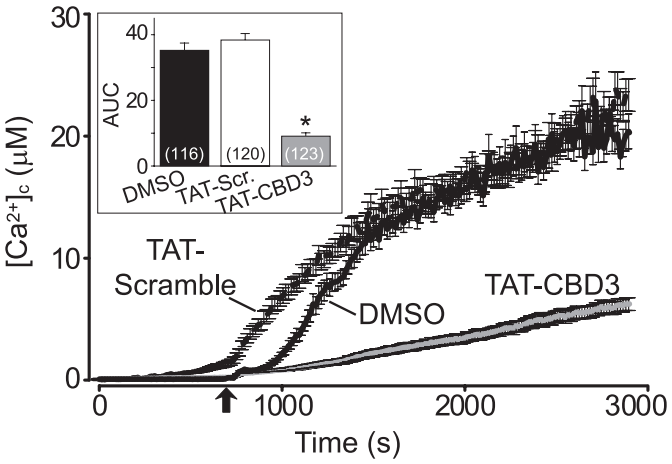

FIGURE 5. **TAT-CBD3 greatly reduces glutamate-induced DCD.** $[Ca^{2+}]_c$ was monitored in E18–19 cortical neurons after prolonged exposure to 200 μM glutamate + 20 μM glycine using the Ca^{2+}-sensitive Fura-2FF. Neurons were treated with vehicle (0.05% DMSO), 10 μM TAT-Control, or TAT-CBD3 for 10 min prior to stimulation with Glu/Gly. The *arrow* indicates the time of Glu/Gly application. The *inset graph* displays the average area under the curve (*AUC*) in arbitrary units. Values represent $n = 116–123$ cells obtained from two separate experiments for each treatment. *Error bars*, S.E.

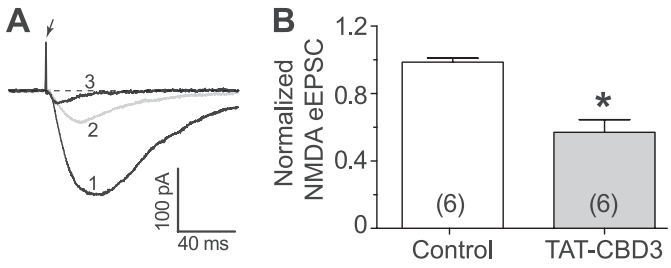

FIGURE 6. **Attenuation of NMDA receptor-mediated synaptic currents by TAT-CBD3 in cortical neurons.** *A*, representative recordings from a cortical neuron showing overlaid traces of a base-line control (*1*), TAT-CBD3 perfused (20 μM, 10 min) (*2*), and following the addition of NMDA antagonist (RS)-3-(2-Carboxypiperazin-4-yl)-propyl-1-phosphonic acid (RS)CPP)) (1 μM) (*3*). The *arrow* represents a stimulation artifact. Holding potential was −60 mV. *B*, pooled data displaying normalized NMDA-mediated current in control and after perfusion with TAT-CBD3 (20 μM) perfusion. Data are expressed as mean ± S.E. (*error bars*) ($n = 6$). The addition of TAT-CBD3 caused a significant reduction of NMDA-mediated eEPSC from cortical neurons (*, $p < 0.01$ *versus* control, Student's *t* test).

Because Ca^{2+} entry is an early event in signaling, we hypothesized that TAT-CBD3 may affect cleavage by reducing Ca^{2+} influx in response to glutamate. During prolonged exposure to glutamate, neurons lose their ability to buffer the large influx of Ca^{2+}, resulting in accumulation of toxic levels of $[Ca^{2+}]_c$, a phenomenon known as delayed calcium deregulation (DCD) (47). To test if TAT-CBD3 alters DCD following glutamate application, the Ca^{2+}-sensitive dye Fura-2FF was used to monitor $[Ca^{2+}]_c$. Neurons were incubated with vehicle (0.05% DMSO) or 10 μM TAT peptides for 10 min prior to a 200 μM glutamate + 20 μM glycine challenge (Fig. 5). This stimulation led to a sustained increase in $[Ca^{2+}]_c$ throughout the time course of the experiment. Both vehicle and TAT-Control displayed similar increases in $[Ca^{2+}]_c$ during the prolonged exposure to glutamate. In contrast, TAT-CBD3 showed a significant decrease in $[Ca^{2+}]_c$ compared with vehicle and TAT-Control. The changes in $[Ca^{2+}]_c$ following glutamate stimulation, represented by average area under the curve, were decreased by a 78 and 75% compared with that observed in TAT-Control and vehicle-treated neurons, respectively (Fig. 5, *inset*). Because we previously demonstrated an interaction between CRMP2 and N-type voltage-gated calcium channels (CaV2.2) (16), we next tested if these channels could contribute to DCD using the CaV2.2-selective blocker ω-conotoxin GVIA (ω-CTX). Incubation with ω-CTX (1 μM) alone did not attenuate the glutamate-induced DCD compared with vehicle (supplemental Fig. 2). The decrease in DCD and Ca^{2+} influx observed in neurons pretreated with TAT-CBD3 supports our hypothesis that TAT-CBD3 decreases glutamate-stimulated Ca^{2+} influx. These findings suggest that the neuroprotective effect of TAT-CBD3 as well as the decrease in calpain cleavage of CRMP2 may occur due to decreased Ca^{2+} influx in the face of glutamate stimulation.

TAT-CBD3 Reduces Cortical NMDAR-mediated eEPSCs—The efficacy of TAT-CBD3 in reducing glutamate-induced DCD suggests that it may reduce postsynaptic activation. In order to investigate this possibility, we sought to measure eEPSCs in cortical neurons. We specifically chose NMDAR-mediated eEPSCs because it has previously been shown that CRMP2 interacts with and modulates NMDARs (12, 13). Using cortical slices which contain intact synapses from adult rats, NMDAR-mediated eEPSCs were isolated by pharmacologically blocking $GABA_{A/B}$ receptors along with AMPA and kainate receptors, as described under "Experimental Procedures." NMDAR-mediated eEPSCs from layer V cortical neurons were recorded following stimulation with an electrode positioned ~500 μm from the neuron being recorded. Using this configuration, peak eEPSCs were stable for 30 min with stimulation occurring every 2 min (Fig. 6*A*, *1*). Peak eEPSCs were recorded following perfusion with 20 μM TAT-CBD3; an example trace at 10 min after continual perfusion of the peptide is shown (Fig. 6*A*, *2*). At the end of every experiment, the NMDAR-selective anatagonist CPP (1 μM) was perfused to verify that the recordings were NMDAR-mediated eEPSCs (Fig. 6*A*, *3*). Perfusion of ACSF containing TAT-CBD3 led to a 50% decrease in eEPSCs compared with perfusion of control ACSF alone ($p < 0.05$, Student's *t* test, $n = 6$; Fig. 6*B*). This decrease in eEPSCs suggests that TAT-CBD3 targets NMDARs and works to reduce their activity. Furthermore, this validates that TAT-CBD3 can effectively target native postsynaptic responses.

TAT-CBD3 Does Not Alter Total Surface Expression of NR2B—Recent work from our laboratory has elaborated on the interaction between CRMP2 and presynaptic calcium channels positioning CRMP2 as a modulator of channel trafficking leading to changes in Ca^{2+} currents (16, 17). Because two recent studies showed an association of NMDARs with CRMP2 and possible regulation of cell surface expression of the NR2B-containing NMDARs by CRMP2 (12, 13), we tested if NMDARs are affected by the CBD3 peptide. Additionally, we focused on the NR2B subunit because it appears to be the dominant subunit implicated in excitotoxicity in young cortical neuron cultures (48–50). To monitor surface expression of the NR2B-containing NMDARs, neurons were pretreated for 10 min with a 10 μM concentration of either TAT peptide followed by a 30-min stimulation with Glu/Ser and then subjected to biotinylation of surface proteins either 30 min, 1 h, or 2 h after stimulation.

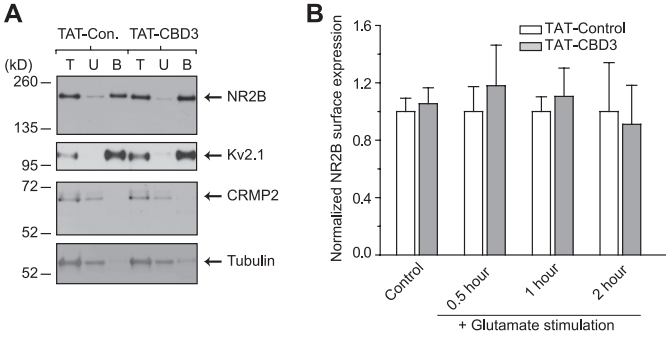

FIGURE 7. **TAT-CBD3 does not alter surface NR2B expression.** *A*, representative immunoblots with the indicated antibodies of total lysates (*T*), unbiotinylated fractions (*U*), and biotinylated fractions (*B*) prepared from neurons exposed to TAT-Control or TAT-CBD3 (10 μM each). *B*, summary of biotinylated (surface) NR2B protein, calculated by densitometry from two experiments. Values were normalized to time-matched TAT-Control conditions (n = 6–11 each). Neurons were left untreated (control) or stimulated for 30 min with Glu/Ser followed by biotinylation 0.5–2 h later. Levels of surface NR2B were not different in any of the conditions tested ($p > 0.05$; Student's t test).

Control neurons were treated with peptide for 10 min and then incubated for 30 min without stimulation before surface proteins were biotinylated. NR2B was mainly detected in the streptavidin-enriched biotinylated fraction (*B*) with trace amounts in the unbound fraction (*U*), consistent with a surface-expressed receptor (Fig. 7*A*). As a control, the surface expression of the voltage-gated potassium channel 2.1 (Kv2.1) was also found primarily in the biotinylated fraction, consistent with our previous report that CRMP2 does not affect Kv channel trafficking (17). As expected, the cytosolic proteins CRMP2 and β-tubulin were present in the unbound fraction with little to none detected in the biotinylated fractions. NR2B surface expression was calculated as the ratio of biotinylated to total NR2B and then normalized to the ratio observed in neurons treated with TAT-Control for the times indicated. There was no difference in the amount of surface-expressed NR2B between TAT-Control- and TAT-CBD3-treated neurons in unstimulated neurons or neurons stimulated for 30 min with Glu/Ser (Fig. 7*B*). Although calpain-cleaved NR2B can remain on the membrane following excitotoxicity-induced cleavage (51–54), this was not the case in our experiments because 1) no detectable cleavage of NR2B *in vitro* was observed in our model of neuronal excitotoxicity up to 2 h following stimulation (Fig. 2, *A* and *B*), and 2) the cleaved NR2B form was recognized by the antibody used for these experiments (supplemental Fig. 3). Taken together, these results suggest that TAT-CBD3 does not alter surface expression of total NR2B.

TAT-CBD3 Reduces NR2B Surface Expression in Dendritic Spines—Because biotinylation experiments do not address potential localized or spatially restricted changes in surface expression of a protein, we turned to the approach of using the pH-sensitive GFP SEP to monitor NR2B surface expression (55). SEP fluoresces 20-fold brighter in a neutral pH *versus* acidic or basic conditions; as proteins on the surface (high fluorescence, pH ~7.5) are internalized (low fluorescence, pH ~5.5), a strong reduction in fluorescence is observed. The fluorescence of SEP fused to the extracellular domain of NR2B (NR2B-SEP) can therefore be used to observe changes in NR2B-SEP-containing NMDARs on the plasma membrane (56). Neurons expressing NR2B-SEP were visualized using confocal fluorescent microscopy as small punctate structures on dendrites (Fig. 8*A*), consistent with previous reports showing clustering of NMDARs in dendritic spines (57, 58). Following acquisition of a 10-min period of base line, neurons were incubated with peptides for 20 min while continually measuring NR2B-SEP fluorescence. At the end of every experiment, neurons were treated with a pulse of acetic acid. This drop in pH (to ~5.5) caused a nearly complete loss of fluorescence and verified that the pH sensitivity of SEP was not altered during the course of the experiment. Incubation of neurons with 10 μM TAT-Control showed no significant change in fluorescence at 20 min compared with vehicle. In contrast, incubation with 10 μM TAT-CBD3 caused a ~60% reduction in NR2B-SEP fluorescence (Fig. 8*B*). This result suggests that CBD3 can alter dendritic surface NMDARs by inducing internalization of NR2B.

Because NMDAR activity has been linked to surface expression (59–61), we tested if inhibition of NMDAR activity could affect TAT-CBD3-induced NR2B internalization. The concomitant addition of the NMDAR antagonist MK801 (50 μM) with 10 μM TAT-CBD3 completely prevented the TAT-CBD3-induced reduction in NR2B-SEP fluorescence observed at 20 min following peptide/drug application (Fig. 8*C*). Treatment with 50 μM MK801 alone had no effect on NR2B-SEP fluorescence. These results suggest that internalization of NMDARs induced by TAT-CBD3 requires an active NMDAR.

Whereas biotinylation experiments showed that surface expression of NR2B is not altered following TAT-CBD3 exposure, NR2B-SEP fluorescence experiments showed reduced NR2B surface expression in dendrites upon treatment with TAT-CBD3. To address the incongruity between these results, we measured NR2B-SEP fluorescence in cell bodies of neurons following treatment with TAT peptides (Fig. 8*D*). NR2B-SEP fluorescence was similar in somas following application of TAT-CBD3 compared with TAT-Control (Fig. 8*E*). The finding that somatic NR2B surface expression is unaltered may explain why no reduction in total NR2B surface expression was observed in biotinylation experiments. Collectively, these observations suggest that TAT-CBD3 induces specific internalization of dendritic NR2B receptors without altering somatic receptors.

TAT-CBD3 Decreases NMDA-stimulated Ca^{2+} Influx in an Activity-dependent Manner—Based on the above observations that TAT-CBD3 down-regulates NR2B in an activity-dependent manner, we next asked if this down-regulation led to a decrease in NMDAR activity by measuring Ca^{2+} influx in response to NMDA. Changes in $[Ca^{2+}]_c$ were monitored using the high affinity Ca^{2+} dye Fura-2 after stimulating neurons with 50 μM NMDA + 100 μM glycine. A sharp increase in $[Ca^{2+}]_c$ was observed when NMDA was applied, which returned to base line upon NMDA removal. When vehicle (DMSO) was applied during the interim between the three NMDA stimulations, no change in $[Ca^{2+}]_c$ amplitude was observed (Fig. 9*A*). However, when neurons were treated with 10 μM TAT-CBD3 during this interim period, the second and third responses to NMDA were strongly attenuated (Fig. 9*B*). This decrease in NMDA response is consistent with internalization of NMDARs observed in the NR2B-SEP imaging experiments.

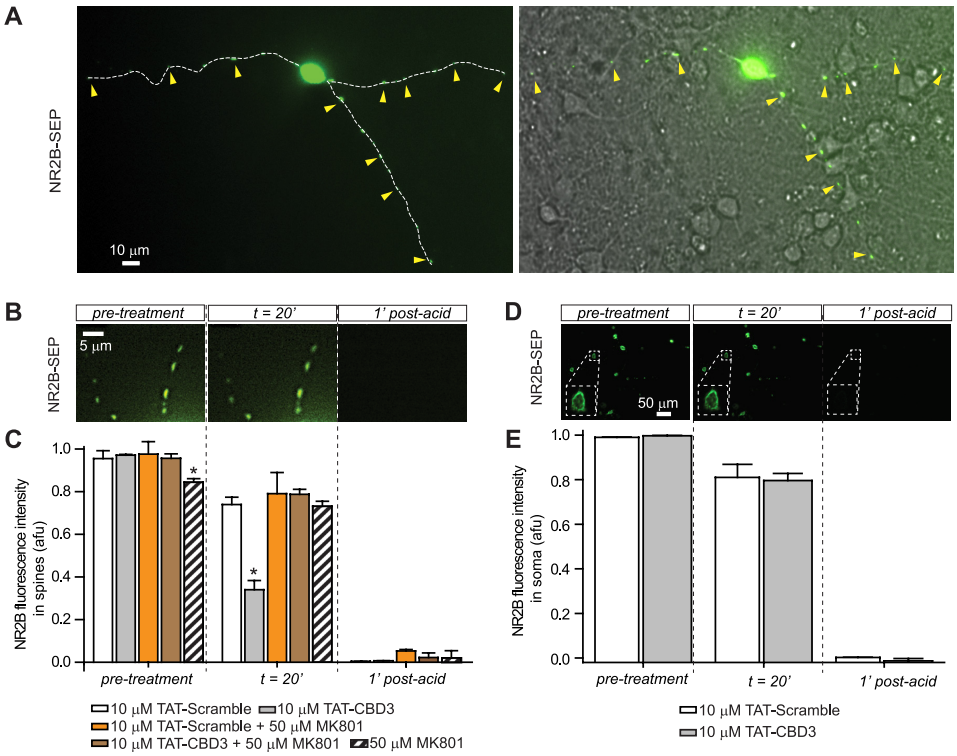

FIGURE 8. **TAT-CBD3 induces activity-dependent down-regulation of NR2B surface expression in dendritic spines.** Representative deconvolved fluorescent images of surface-expressed NR2B-SEP on dendritic spines (*A* and *B*) or soma (*D*) of transfected neurons before, 20 min after application of TAT-Control, and 1 min after application of a short acid pulse (pH 5.0). A differential interference contrast image overlaid with a fluorescent image illustrating dendritic spines rich in NR2B (*yellow arrowheads*) is shown in *A* (*right*). Shown are average NR2B-SEP fluorescence intensities in spines (*C*) or soma (*E*) in the presence of MK801 alone or peptides alone or in the presence of peptides and MK801 at the times indicated. Each condition represents 37–70 spines from three experiments or 32–34 soma. *, significant difference compared with time-matched TAT-Control ($p < 0.05$; ANOVA for spines and Student's *t* test for soma). The *ordinate* represents average intensity in arbitrary fluorescent units (*afu*). *Scale bars* are as indicated. *Error bars*, S.E.

Having confirmed that TAT-CBD3 not only reduces surface expression of NMDARs but also reduces the NMDA-initiated Ca^{2+} influx, we next asked if the latter effect was also activity-dependent using the reversible NMDAR inhibitor (2*R*)-amino-5-phosphonopentanoate (AP-5) (62). When NMDA was applied in the presence of 100 μM AP-5, no $[Ca^{2+}]_c$ increase was observed (Fig. 9*C*). However, upon washout of AP-5, NMDA application elicited a $[Ca^{2+}]_c$ increase slightly greater in magnitude than that seen before AP-5 application. NMDA-stimulated $[Ca^{2+}]_c$ increase was completely blocked when TAT-CBD3 and AP-5 were co-applied but returned following washout of AP-5 (Fig. 9*D*). The ratio of the second to first NMDA-induced Ca^{2+} peak (P2/P1) for vehicle-treated neurons was 1.05 ± 0.09, whereas incubation with 10 μM TAT-CBD3 reduced the P2/P1 ratio to 0.25 ± 0.03 (Fig. 9*F*). The ratio of the third to first Ca^{2+} peak (P3/P1) for TAT-CBD3 neurons was 0.33 ± 0.03, suggesting only a minimal recovery of active surface NMDARs. Co-application of TAT-CBD3 with 100 μM AP-5 led to a P2/P1 ratio of 0.19 ± 0.03 and a P3/P1 of 0.93 ± 0.08, indicating recovery of active surface NMDARs. To rule out the possibility that Ca^{2+} entry via voltage-gated Ca^{2+} channels could account for these effects, we performed experiments with ω-CTX which showed no inhibition of NMDA-mediated Ca^{2+} increase (P2/P1 = 0.99 ± 0.03), suggesting lack of involvement of at least N-type Ca^{2+} channels (Fig. 9*E*). These findings show that inhibition of NMDARs prevents the TAT-CBD3-mediated decrease in NMDA-initiated $[Ca^{2+}]_c$ increase. Collectively, the NR2B-SEP imaging and $[Ca^{2+}]_c$ experiments strongly support the conclusion that NMDAR internalization following TAT-CBD3 treatment is activity-dependent.

We next asked if TAT-CBD3 inhibition of NMDAR-mediated Ca^{2+}-influx was CRMP2-dependent. Neurons were transfected with CRMP2 siRNA + GFP at 5 DIV, and then Ca^{2+} imaging was performed using a two-pulse NMDA protocol at 7 DIV. Neurons treated with CRMP2 siRNA exhibited reduced inhibition of NMDAR-mediated Ca^{2+} influx by TAT-CBD3 (P2/P1 = 0.60 ± 0.09) *versus* untransfected controls (P2/P1 = 0.29 ± 0.06, $n = 7$, $p < 0.05$, Student's *t* test). This result suggests that the efficacy of TAT-CBD3 in reducing NMDAR-mediated Ca^{2+}-influx is CRMP2-dependent, supporting the notion that TAT-CBD3 antagonizes a function of CRMP2.

TAT-CBD3 Inhibits NMDAR-induced Current in Hippocampal Neurons—The attenuation of NMDA-stimulated Ca^{2+} influx suggests that TAT-CBD3 acts on the NMDAR. To further validate that TAT-CBD3 inhibits NMDARs, we tested if TAT-CBD3 could inhibit NMDA-evoked currents in primary neurons. NMDAR currents were recorded from rat hippocampal neurons (DIV 7–11) using whole cell voltage clamp electrophysiology by stimulating with 50 μM NMDA for 2 s with a 30-s interval between stimulations (Fig. 10*A*). Following 5 min of stable NMDA-stimulated responses (<5% change between peaks), neurons were perfused with 10 μM TAT-CBD3. TAT-CBD3 induced rapid and strong inhibition of NMDA currents with ~70% block after 5 min (Fig. 10*B*). Washout with bath

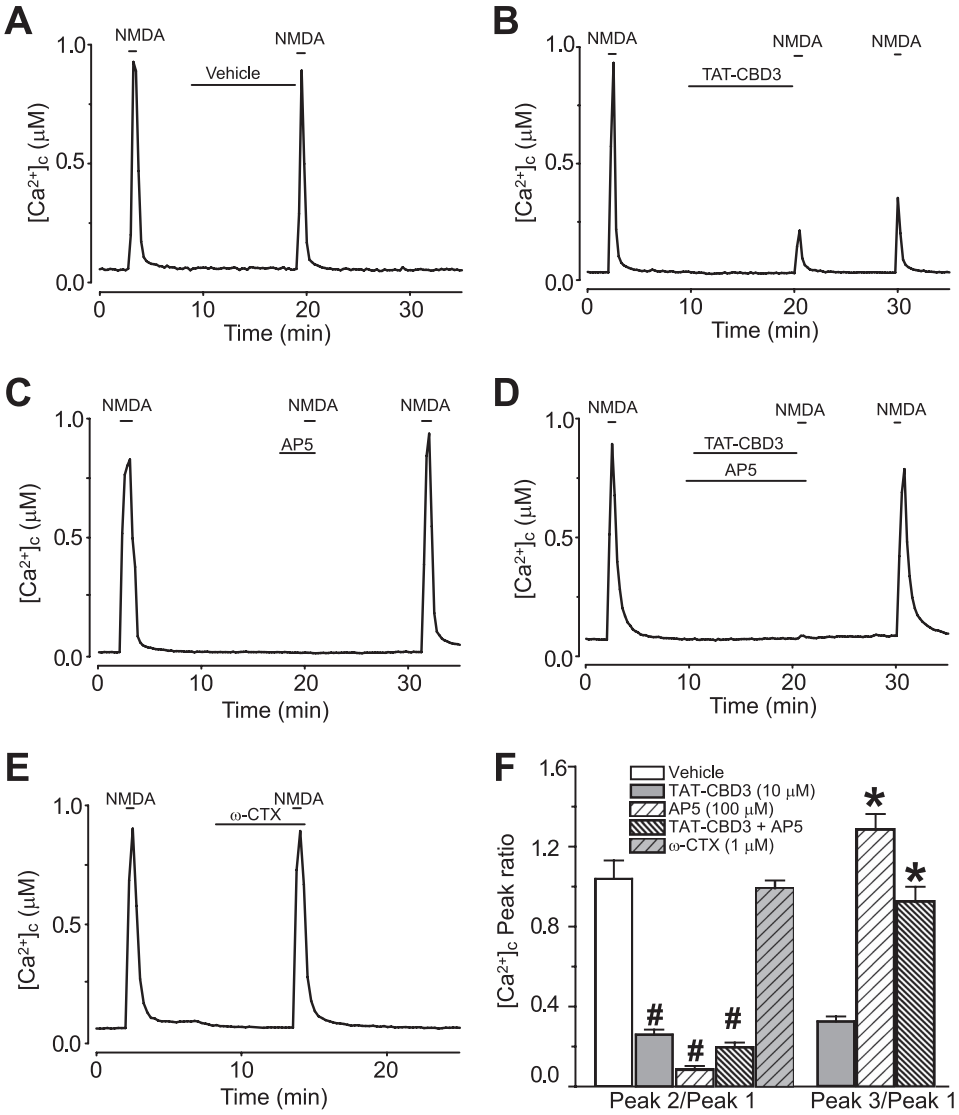

FIGURE 9. **TAT-CBD3 decreases NMDA-stimulated Ca^{2+} influx in an activity-dependent manner.** *A*, $[Ca^{2+}]_c$ was monitored in E18–19 cortical neurons using the Ca^{2+}-sensitive dye Fura-2 following application of 50 μM NMDA + 100 μM glycine. Following application of NMDA, neurons were treated with vehicle (0.05% DMSO) for 10 min and then challenged again with NMDA, before a final application ~20 min following the first one. *B–E*, in addition to vehicle, neurons were also treated with either 10 μM TAT-CBD3, 100 μM AP-5, TAT-CBD3 + AP-5, or 1 μM ω-conotoxin GVIA during the 10 min in the interim between the first and second NMDA applications. *E*, inhibition of N-type Ca^{2+} channels with 1 μM ω-CTX did not affect NMDA-evoked $[Ca^{2+}]_c$ increases. *F*, *bar graph* summarizing the ratios of the second and third NMDA applications to the first for the various treatment conditions. All values represent at least 95 cells from 2–3 separate experiments. Statistical significance compared with vehicle-treated neurons is denoted by an *asterisk* for P2/P1 ($p < 0.05$), whereas the *number sign* denotes significance compared with TAT-CBD3-treated neurons for P3/P1 ($p < 0.05$, one-way ANOVA). *Error bars*, S.E.

solution lacking TAT-CBD3 led to partial recovery of NMDA currents after 10 min. These findings place TAT-CBD3 as a modulator of NMDARs and show that TAT-CBD3 directly inhibits NMDA currents.

TAT-CBD3 Protects Neurons against Traumatic Brain Injury—To assess if TAT-CBD3 has neuroprotective effects *in vivo*, we employed a CCI model of moderate TBI (36, 38, 39, 63). Five minutes following TBI, mice received intraperitoneal injection of TAT-CBD3 or saline. Using FITC-TAT-CBD3, we first confirmed that the peptide was taken up by neurons in TBI-affected regions following an intraperitoneal injection (supplemental Fig. 4). Neuronal death was assessed using FJB stain to label dying neurons (40) at 24 h following TBI because this time represents the peak of cell death within the hippocampus (63). Dying neurons were mainly observed in the ipsilateral neocortex around the lesion area (Fig. 11, *A* and *B*) and in the ipsilateral hippocampus (Fig. 11, *C–F*). In the hippocampus, there were ~50% fewer dying neurons in animals injected with TAT-CBD3 compared with those injected with saline ($p < 0.05$; Student's *t* test; Fig. 11*G*). Within the hippocampus of TAT-CBD3-injected animals, granule cell layer neurons exhibited a significantly lesser density of death compared with saline-injected animals (Fig. 11, *E*, *F*, and *H*). There was no significant difference in the density of dying neurons from CA1 and CA3 regions between saline- and TAT-CBD3-injected animals despite evidence of FITC-TAT-CBD3 labeling in neurons in the ipsilateral cortex (Fig. 11*G*). No FJB-positive cells were observed in the contralateral cortex (data not shown). These results suggest that TAT-CBD3 protects hippocampal granular cells *in vivo*.

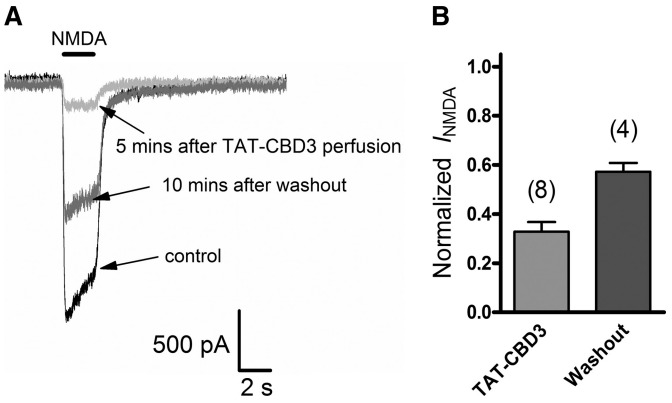

FIGURE 10. **TAT-CBD3 decreases NMDA induced current in rat hippocampal neurons.** *A*, representative traces from a single neuron, showing a control NMDA trace evoked by 50 μM NMDA (see "Experimental Procedures"), NMDA current after a 5-min perfusion of 10 μM TAT-CBD3, and NMDA current after a 10-min washout of TAT-CBD3. *B*, *bar graph* summarizing the effect of TAT-CBD3 on NMDA current of eight individual cells; four of those cells lasted long enough to finish a 10-min washout period and partially recovered from TAT-CBD3 effect. *Error bars*, S.E.

DISCUSSION

In this study, we describe the neuroprotective effects of a novel peptide (CBD3) derived from the CRMP2 protein. Knockdown of CRMP2 itself was neuroprotective (Fig. 12). However, knockdown of CRMP2 was not completely neuroprotective because additional protection was conferred by treatment with TAT-CBD3 peptide, raising the possibility that the TAT-CBD3 peptide may target additional proteins with a similar motif. Because CRMP2 has at least 20 binding partners (15), it is possible that TAT-CBD3 may target other CRMP2 binding partners, additionally preventing binding of CRMP2 to other targets, which include proteins involved with cytoskeletal structure, dynamic cytoskeletal reorganization, axonal transport, vesicle trafficking, endocytosis, or synaptic vesicle targeting (for a review, see Ref. 15). It is difficult to predict which of these proteins may be affected because the regions of CRMP2 required for binding to many of these targets are unknown. Therefore, it is conceivable that the additional neuroprotection observed with TAT-CBD3 treatment compared with CRMP2 knockdown may be due to decreased binding to other targets.

Incubation with TAT-CBD3 protected neurons from glutamate toxicity, decreased surface expression of NR2B receptors at dendritic spines, and reduced NMDAR-mediated Ca^{2+} influx. TAT-CBD3 was also found to inhibit NMDAR-mediated currents in slice recordings and in cultured neurons. Although CRMP2 was originally discovered as a mediator of axon guidance and outgrowth, recent evidence from our laboratory has suggested that CRMP2 is also important in calcium regulation (16) and in excitotoxicity signaling (13, 22). Our results, for the first time, establish CRMP2 signaling as a *bona fide* target for prevention of glutamate toxicity and the loss of hippocampal neurons in a model of TBI. The apparent mechanism of action for the neuroprotective effect of TAT-CBD3 in glutamate toxicity is via attenuation of toxic Ca^{2+} influx through NMDARs. TAT-CBD3 probably increased survival of hippocampal neurons following TBI by reducing toxic glutamate-induced Ca^{2+} influx through NMDARs. These mechanisms together suggest that CRMP2 interacts with and modulates NR2B-containing NMDARs (12, 13).

Initial support for CRMP2 as a potential target in neurotoxicity arose from studies showing cleavage of CRMP2 by calpain following various forms of neurotoxicity, including focal ischemia (13, 20, 23–26). These findings led us to hypothesize that TAT-CBD3 may alter calpain cleavage of CRMP2, which in turn may be neuroprotective in a cell-based excitotoxic injury model and a murine model of neurotrauma. Consistent with our hypothesis, we observed strong neuroprotection by TAT-CBD3 in both models. Despite the finding that TAT-CBD3 also reduced calpain cleavage of CRMP2, this is probably not the mechanism of TAT-CBD3-induced neuroprotection because no reduction in cleavage occurred when TAT-CBD3 was added to *in vitro* cleavage experiments. Rather, it appears that the reduction in cleavage is due to a reduction in glutamate-induced Ca^{2+} influx.

In addition to CRMP2, cleavage of other members of the CRMP family of proteins has been implicated in neurotoxicity. Collectively, it appears that cleavage of CRMP3 and CRMP4 is detrimental to neuronal survival, whereas cleavage of CRMP2 may be neuroprotective (13, 64, 65). The possible effect that cleavage of CRMP1 and -5 may have on neuronal survival is at present unclear. The CBD3 region of CRMP2 shares 80% identity with CRMP3 but only 46 and 40% identity with CRMP-4 and CRMP1, respectively. Given the sequence disparity between the CBD3 regions for CRMP1 to -4, it would be interesting to test if these peptides also have neuroprotective properties. Furthermore, the use of these CBD3 homologues might enable identification of specific residues required for neuroprotection.

A recent study reported that overexpression of a "cleaved" CRMP2 construct, lacking amino acids 509–572, which are cleaved by calpain, reduced the responsiveness of neurons to glutamate and increased neuronal survival following glutamate-induced toxicity (13). The authors concluded that accumulation of this artificially cleaved CRMP2 product leads to a reduction of surface NMDARs, presumably accounting for the observed neuropreservation. Their study, however, did not examine whether cleavage of *endogenous* CRMP2 could also be neuroprotective. In this study, we initially set out to determine if TAT-CBD3 altered calpain cleavage of CRMP2 and neuronal survival following excitotoxicity. Although our results show that TAT-CBD3 reduced cleavage of CRMP2 and was neuroprotective following an excitotoxic insult, this relationship may not be a causal one because it appears that TAT-CBD3-mediated attenuation of NMDAR-mediated Ca^{2+} influx is the likely cause for both neuroprotection and prevention of calpain cleavage of CRMP2 (Fig. 12). These findings position CRMP2 as an important novel modulator of both ligand-gated (*i.e.* NMDARs) as well as voltage-gated calcium channels (16, 17).

Incubation with TAT-CBD3 greatly attenuated DCD during prolonged glutamate exposure as well as reduced Ca^{2+} influx following NMDA application. Perhaps most interesting, however, is the finding that TAT-CBD3 induces activity-dependent internalization of NMDARs because inhibitors of NMDARs (MK801 and AP-5) prevented TAT-CBD3 modulation of NMDARs. TAT-CBD3-mediated internalization appears to occur quite rapidly because ~74% of the NMDA-mediated

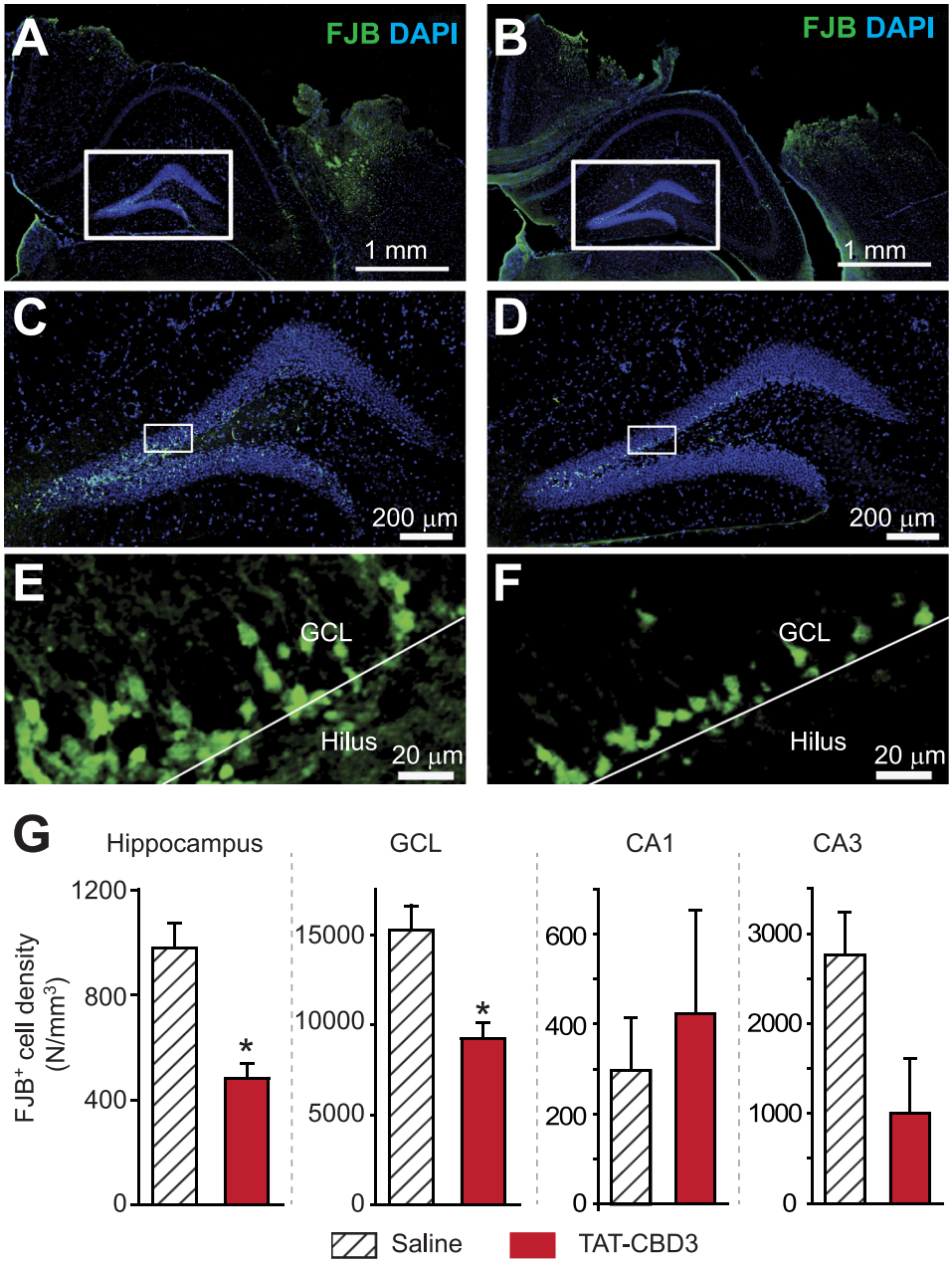

FIGURE 11. **TAT-CBD3 protects against neuronal death following moderate traumatic brain injury.** Five min following TBI, mice received intraperitoneal injection of either saline (*A*, *C*, and *E*) or TAT-CBD3 (*B*, *D*, and *F*). Shown are representative images from slices illustrating dying neurons stained with FJB (*green*) and nuclei of all cells counterstained with DAPI (*blue*) 24 h after injury. *A* and *B*, ipsilateral side of cortex with FJB and DAPI staining 24 h after TBI surgery. *C* and *D*, hippocampal dentate gyri enlarged from *A* and *B*. *E* and *F*, granule cell layer (*GCL*) enlarged from *C* and *D*. The boundary between the GCL and the hilus is denoted by the *white line*. *G*, summary of the density of dying neurons (in number (*N*)/mm^3) within the hippocampus, granular cell layer, and CA1 and CA3 regions. Data are from 98 slices (from six saline-injected animals) and 78 slices (from four TAT-CBD3-injected animals). *Error bars*, S.E.

Ca^{2+} influx was lost after a 10-min exposure to TAT-CBD3. This is considerably greater than the glycine/D-serine-induced 30% decrease in NMDA currents observed within 10 min (66). Although a biochemical interaction between NMDARs and CRMP2 has been reported, the specific regions mediating the interaction are currently unknown (12); nor is it known if the interaction is direct or via other protein(s). Given that CRMP2 has been recently implicated in regulating trafficking of calcium channels, including NMDARs (13), it is likely that intracellular domains of NMDARs may be involved, particularly those reported to be involved in trafficking/internalization. Possible mechanisms for TAT-CBD3-induced trafficking/internalization could include phosphorylation of the NMDAR or interaction with AP-2 adaptor proteins in the NR2B C terminus (67–69). Previous work has shown that CRMP2 interacts with α-adaptin (an AP-2 subunit) and modulates endocytosis of the cell adhesion protein L1, suggesting that CRMP2 could potentially modulate NR2B endocytosis through an interaction with AP-2 (70). TAT-CBD3-initiated NMDAR removal from the membrane could occur through an interaction with these or as yet unknown NMDAR trafficking pathways. The specific removal of NR2B receptors from spines suggests that TAT-CBD3 could be targeting a synaptic trafficking pathway, possibly explaining why somatic receptors are not affected.

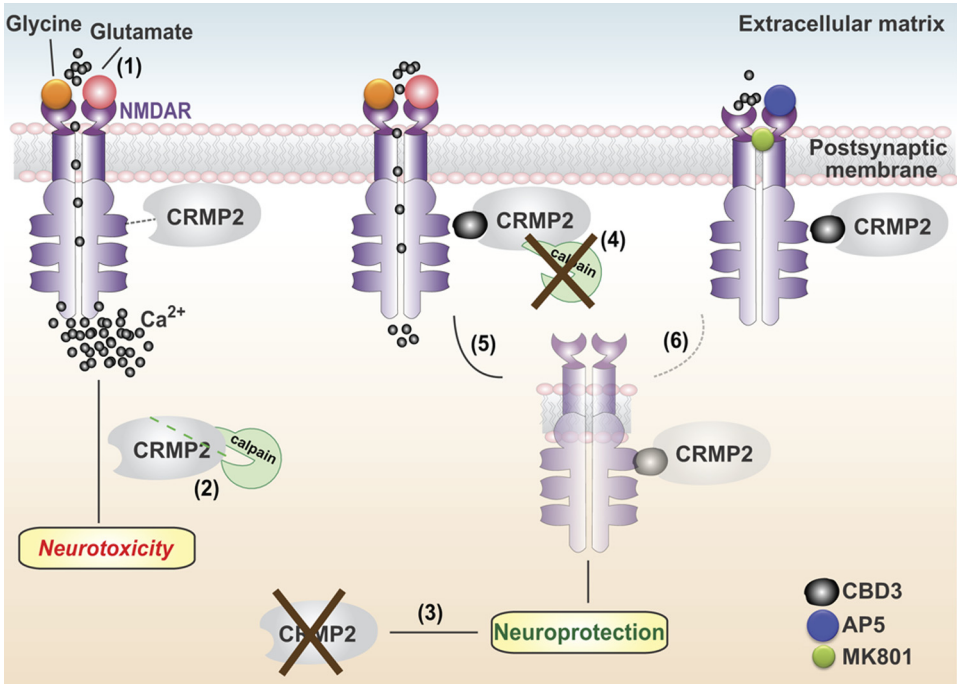

FIGURE 12. **Putative mechanism of CRMP2 and TAT-CBD3 action in neuroprotection.** *1*, engagement of the glutamate or glycine binding sites on the extracellular face of the NMDAR allows influx of Na^+ and Ca^{2+} ions. Hyperactivation of NMDARs, such as that occurring in traumatic brain injury, leads to a massive influx of Ca^{2+} ions that, in turn, leads to the overactivation of several deleterious enzymes and signaling pathways that harm neurons or lead to cell death (excitotoxicity). *2*, this increase in intracellular Ca^{2+} leads to activation of the Ca^{2+}-activated protease calpain, which cleaves various substrates, including CRMP2. *3*, we observed that lentivirus-mediated knockdown of CRMP-2 reduces neuronal death following excitotoxicity. *4*, the CRMP-2 peptide CBD3 greatly attenuates Ca^{2+} influx through NMDARs and subsequently reduces calpain-mediated cleavage of CRMP-2. *5*, CBD3 also induces internalization of NMDARs, leading to sparing of neurons following an excitotoxic insult. *6*, that NMDAR antagonists (MK801 and AP-5) prevent both CBD3-induced NMDAR internalization and CBD3-mediated reduction in Ca^{2+} influx implies that the CBD3 mechanism of action on NMDARs is probably activity-dependent. Collectively, these findings suggest that CRMP2 (as well as a short peptide derived from it (*i.e.* CBD3)) is an important determinant for neuronal survival following glutamate exposure and could therefore be a target for neuroprotection.

The neuroprotective efficacy of TAT-CBD3 in the CCI model of TBI underscores that modulation of NMDARs by CRMP2 is physiologically important. TAT-CBD3 administered systemically within minutes of injury protected ~50% of the neurons in the granular cell layer within the hippocampus against TBI and protected against an excitotoxic stimulation *in vitro* at 30 min postchallenge, supporting the notion that TAT-CBD3 works in the early phase of neuronal death observed following excitotoxic insults.

Despite several studies showing the neuroprotective efficacy of NMDAR inhibitors in cell culture and animal models of excitotoxicity, clinical trials for NMDAR inhibitors have been largely unsuccessful (7, 71), with only limited successes (8, 9). The failure of these trials has been attributed, in part, to the negative side effects of completely blocking NMDARs. Therefore, an alternative approach that may be more therapeutically beneficial is to modulate, rather than completely block, NMDARs to reduce excitotoxicity. In this regard, TAT-CBD3 is an exciting new tool for neuroprotection in excitoxicity because it selectively reduces NMDAR surface expression in dendrites and attenuates Ca^{2+} influx without completely ablating NMDA/glutamate responses. This strategy could be especially helpful for reducing the excitotoxic death of neurons without preventing the "normal" postinjury glutamate responses, which are important for continued survival of glutamatergic neurons (6).

In conclusion, we have identified a novel neuroprotective peptide derived from the protein CRMP2 (72). This peptide appears to work by inhibiting NMDARs and inducing dendritic spine NMDAR internalization, culminating in a reduction of glutamate-induced DCD and NMDA-stimulated Ca^{2+} influx. These findings show that CRMP2 is not only involved in glutamate-mediated neurotoxicity but may be effectively targeted to prevent excitotoxicity-mediated neuronal death.

Acknowledgments—We thank Dr. Roberto Malinow for the SEP-NR2B construct (Addgene, Cambridge, MA); Jessica Head, Michael Due, Matthew Ripsch, and Bo Myung Cheon for technical assistance; Dr. May Khanna for helpful comments and Dr. Philip Johnson for help with the illustration.

REFERENCES

1. Choi, D. W. (1985) *Neurosci. Lett.* **58,** 293–297
2. Park, C. K., Nehls, D. G., Graham, D. I., Teasdale, G. M., and McCulloch, J. (1988) *Ann. Neurol.* **24,** 543–551
3. Faden, A. I., Demediuk, P., Panter, S. S., and Vink, R. (1989) *Science* **244,** 798–800
4. Muir, K. W., and Lees, K. R. (2003) *Cochrane Database Syst. Rev.* CD001244
5. Ikonomidou, C., Stefovska, V., and Turski, L. (2000) *Proc. Natl. Acad. Sci. U.S.A.* **97,** 12885–12890
6. Ikonomidou, C., and Turski, L. (2002) *Lancet Neurol.* **1,** 383–386
7. Muir, K. W. (2006) *Curr. Opin. Pharmacol.* **6,** 53–60
8. Volbracht, C., van Beek, J., Zhu, C., Blomgren, K., and Leist, M. (2006) *Eur. J. Neurosci.* **23,** 2611–2622
9. Sonkusare, S. K., Kaul, C. L., and Ramarao, P. (2005) *Pharmacol. Res.* **51,** 1–17
10. Parsons, C. G., Danysz, W., and Quack, G. (1999) *Neuropharmacology* **38,**

735–767
11. Jain, K. K. (2000) *Expert Opin. Investig. Drugs* **9,** 1397–1406
12. Al-Hallaq, R. A., Conrads, T. P., Veenstra, T. D., and Wenthold, R. J. (2007) *J. Neurosci.* **27,** 8334–8343
13. Bretin, S., Rogemond, V., Marin, P., Maus, M., Torrens, Y., Honnorat, J., Glowinski, J., Prémont, J., and Gauchy, C. (2006) *J. Neurochem.* **98,** 1252–1265
14. Schmidt, E. F., and Strittmatter, S. M. (2007) *Adv. Exp. Med. Biol.* **600,** 1–11
15. Hensley, K., Venkova, K., Christov, A., Gunning, W., and Park, J. (2011) *Mol. Neurobiol.* **43,** 180–191
16. Brittain, J. M., Piekarz, A. D., Wang, Y., Kondo, T., Cummins, T. R., and Khanna, R. (2009) *J. Biol. Chem.* **284,** 31375–31390
17. Chi, X. X., Schmutzler, B. S., Brittain, J. M., Hingtgen, C. M., Nicol, G. D., and Khanna, R. (2009) *J. Cell Sci.* **23,** 4351–4362
18. Wang, Y., Brittain, J. M., Wilson, S. M., and Khanna, R. (2010) *Commun. Integr. Biol.* **3,** 172–175
19. Brittain, J. M., Duarte, D. B., Wilson, S. M., Zhu, W., Ballard, C., Johnson, P. L., Liu, N., Xiong, W., Ripsch, M. S., Wang, Y., Fehrenbacher, J. C., Fitz, S. D., Khanna, M., Park, C. K., Schmutzler, B. S., Cheon, B. M., Due, M. R., Brustovetsky, T., Ashpole, N. M., Hudmon, A., Meroueh, S. O., Hingtgen, C. M., Brustovetsky, N., Ji, R. R., Hurley, J. H., Jin, X., Shekhar, A., Xu, X. M., Oxford, G. S., Vasko, M. R., White, F. A., and Khanna, R. (2011) *Nat. Med.* **17,** 822–829
20. Chung, M. A., Lee, J. E., Lee, J. Y., Ko, M. J., Lee, S. T., and Kim, H. J. (2005) *Neuroreport* **16,** 1647–1653
21. Chen, A., Liao, W. P., Lu, Q., Wong, W. S., and Wong, P. T. (2007) *Neurochem. Int.* **50,** 1078–1086
22. Hou, S. T., Jiang, S. X., Aylsworth, A., Ferguson, G., Slinn, J., Hu, H., Leung, T., Kappler, J., and Kaibuchi, K. (2009) *J. Neurochem.* **111,** 870–881
23. Jiang, S. X., Kappler, J., Zurakowski, B., Desbois, A., Aylsworth, A., and Hou, S. T. (2007) *Eur. J. Neurosci.* **26,** 801–809
24. Touma, E., Kato, S., Fukui, K., and Koike, T. (2007) *Eur. J. Neurosci.* **26,** 3368–3381
25. Zhang, Z., Majava, V., Greffier, A., Hayes, R. L., Kursula, P., and Wang, K. K. (2009) *Cell Mol. Life Sci.* **66,** 526–536
26. Zhang, Z., Ottens, A. K., Sadasivan, S., Kobeissy, F. H., Fang, T., Hayes, R. L., and Wang, K. K. (2007) *J. Neurotrauma* **24,** 460–472
27. Vosler, P. S., Brennan, C. S., and Chen, J. (2008) *Mol. Neurobiol.* **38,** 78–100
28. Hou, S. T., Jiang, S. X., Desbois, A., Huang, D., Kelly, J., Tessier, L., Karchewski, L., and Kappler, J. (2006) *J. Neurosci.* **26,** 2241–2249
29. Shleper, M., Kartvelishvily, E., and Wolosker, H. (2005) *J. Neurosci.* **25,** 9413–9417
30. Hansen, M. B., Nielsen, S. E., and Berg, K. (1989) *J. Immunol. Methods* **119,** 203–210
31. Kennett, S. B., Roberts, J. D., and Olden, K. (2004) *J. Biol. Chem.* **279,** 3300–3307
32. Grynkiewicz, G., Poenie, M., and Tsien, R. Y. (1985) *J. Biol. Chem.* **260,** 3440–3450
33. Pickel, V. M., Colago, E. E., Mania, I., Molosh, A. I., and Rainnie, D. G. (2006) *Neuroscience* **142,** 671–690
34. Molosh, A. I., Johnson, P. L., Fitz, S. D., Dimicco, J. A., Herman, J. P., and Shekhar, A. (2010) *Neuropsychopharmacology* **35,** 1333–1347
35. Khosravani, H., Zhang, Y., Tsutsui, S., Hameed, S., Altier, C., Hamid, J., Chen, L., Villemaire, M., Ali, Z., Jirik, F. R., and Zamponi, G. W. (2008) *J. Cell Biol.* **181,** 551–565
36. Sullivan, P. G., Bruce-Keller, A. J., Rabchevsky, A. G., Christakos, S., Clair, D. K., Mattson, M. P., and Scheff, S. W. (1999) *J. Neurosci.* **19,** 6248–6256
37. Gao, X., and Chen, J. (2009) *J. Neurotrauma* **26,** 1325–1335
38. Hall, E. D., Sullivan, P. G., Gibson, T. R., Pavel, K. M., Thompson, B. M., and Scheff, S. W. (2005) *J. Neurotrauma* **22,** 252–265
39. Brody, D. L., Mac Donald, C., Kessens, C. C., Yuede, C., Parsadanian, M., Spinner, M., Kim, E., Schwetye, K. E., Holtzman, D. M., and Bayly, P. V. (2007) *J. Neurotrauma* **24,** 657–673
40. Schmued, L. C., and Hopkins, K. J. (2000) *Brain Res.* **874,** 123–130
41. Amaral, D. G., and Witter, M. P. (1989) *Neuroscience* **31,** 571–591
42. Schwarze, S. R., Ho, A., Vocero-Akbani, A., and Dowdy, S. F. (1999) *Science* **285,** 1569–1572
43. Mothet, J. P., Parent, A. T., Wolosker, H., Brady, R. O., Jr., Linden, D. J., Ferris, C. D., Rogawski, M. A., and Snyder, S. H. (2000) *Proc. Natl. Acad. Sci. U.S.A.* **97,** 4926–4931
44. Adamec, E., Beermann, M. L., and Nixon, R. A. (1998) *Brain Res. Mol. Brain Res.* **54,** 35–48
45. Czogalla, A., and Sikorski, A. F. (2005) *Cell Mol. Life Sci.* **62,** 1913–1924
46. Lee, M. S., Kwon, Y. T., Li, M., Peng, J., Friedlander, R. M., and Tsai, L. H. (2000) *Nature* **405,** 360–364
47. Nicholls, D. G. (2004) *Curr. Mol. Med.* **4,** 149–177
48. Hardingham, G. E., Fukunaga, Y., and Bading, H. (2002) *Nat. Neurosci.* **5,** 405–414
49. Stanika, R. I., Pivovarova, N. B., Brantner, C. A., Watts, C. A., Winters, C. A., and Andrews, S. B. (2009) *Proc. Natl. Acad. Sci. U.S.A.* **106,** 9854–9859
50. Liu, Y., Wong, T. P., Aarts, M., Rooyakkers, A., Liu, L., Lai, T. W., Wu, D. C., Lu, J., Tymianski, M., Craig, A. M., and Wang, Y. T. (2007) *J. Neurosci.* **27,** 2846–2857
51. Simpkins, K. L., Guttmann, R. P., Dong, Y., Chen, Z., Sokol, S., Neumar, R. W., and Lynch, D. R. (2003) *J. Neurosci.* **23,** 11322–11331
52. Dong, Y. N., Waxman, E. A., and Lynch, D. R. (2004) *J. Neurosci.* **24,** 11035–11045
53. Wu, H. Y., Yuen, E. Y., Lu, Y. F., Matsushita, M., Matsui, H., Yan, Z., and Tomizawa, K. (2005) *J. Biol. Chem.* **280,** 21588–21593
54. Yuen, E. Y., Ren, Y., and Yan, Z. (2008) *Mol. Pharmacol.* **74,** 360–370
55. Miesenböck, G., De Angelis, D. A., and Rothman, J. E. (1998) *Nature* **394,** 192–195
56. Kopec, C. D., Li, B., Wei, W., Boehm, J., and Malinow, R. (2006) *J. Neurosci.* **26,** 2000–2009
57. Craig, A. M., Blackstone, C. D., Huganir, R. L., and Banker, G. (1994) *Proc. Natl. Acad. Sci. U.S.A.* **91,** 12373–12377
58. Kornau, H. C., Schenker, L. T., Kennedy, M. B., and Seeburg, P. H. (1995) *Science* **269,** 1737–1740
59. Barria, A., and Malinow, R. (2002) *Neuron* **35,** 345–353
60. Prybylowski, K., Chang, K., Sans, N., Kan, L., Vicini, S., and Wenthold, R. J. (2005) *Neuron* **47,** 845–857
61. Roche, K. W., Standley, S., McCallum, J., Dune Ly, C., Ehlers, M. D., and Wenthold, R. J. (2001) *Nat. Neurosci.* **4,** 794–802
62. Crunelli, V., Forda, S., and Kelly, J. S. (1983) *J. Physiol.* **341,** 627–640
63. Gao, X., Deng-Bryant, Y., Cho, W., Carrico, K. M., Hall, E. D., and Chen, J. (2008) *J. Neurosci. Res.* **86,** 2258–2270
64. Kowara, R., Chen, Q., Milliken, M., and Chakravarthy, B. (2005) *J. Neurochem.* **95,** 466–474
65. Liu, W., Zhou, X. W., Liu, S., Hu, K., Wang, C., He, Q., and Li, M. (2009) *Proteomics* **9,** 3712–3728
66. Nong, Y., Huang, Y. Q., Ju, W., Kalia, L. V., Ahmadian, G., Wang, Y. T., and Salter, M. W. (2003) *Nature* **422,** 302–307
67. Chung, H. J., Huang, Y. H., Lau, L. F., and Huganir, R. L. (2004) *J. Neurosci.* **24,** 10248–10259
68. Clapp, P., Gibson, E. S., Dell'acqua, M. L., and Hoffman, P. L. (2010) *J. Pharmacol. Exp. Ther.* **332,** 720–729
69. Zhang, S., Edelmann, L., Liu, J., Crandall, J. E., and Morabito, M. A. (2008) *J. Neurosci.* **28,** 415–424
70. Nishimura, T., Fukata, Y., Kato, K., Yamaguchi, T., Matsuura, Y., Kamiguchi, H., and Kaibuchi, K. (2003) *Nat. Cell Biol.* **5,** 819–826
71. Villmann, C., and Becker, C. M. (2007) *Neuroscientist* **13,** 594–615
72. Wilson, S. M., Brittain, J. M., Piekarz, A. D., Ballard, C. J., Ripsch, M. S., Cummins, T. R., Hurley, J. H., Khanna, M., Hammes, N. M., Samuels, B. C., White, F. A., and Khanna, R. (2011) *Channels* (*Austin*), in press